Chapter 7 in the book:
P.A. Kralchevsky and K. Nagayama, "Particles at Fluid Interfaces and Membranes," Elsevier, Amsterdam, 2001; pp. 287–350

CHAPTER 7

LATERAL CAPILLARY FORCES BETWEEN PARTIALLY IMMERSED BODIES

This chapter describes results from theoretical and experimental studies on lateral capillary forces. Such forces emerge when the contact of particles, or other bodies, with a fluid phase boundary causes perturbations in the interfacial shape. The latter can appear around floating particles, semi-immersed vertical cylinders, particles confined in a liquid film, inclusions in the membranes of lipid vesicles or living cells, etc. Except the case of floating particles (see Chapter 8), whose weight produces the meniscus deformations, in all other cases the deformations are due to the surface wetting properties of partially immersed bodies or particles. The "immersion" capillary forces, resulting from the overlap of such interfacial perturbations, can be large enough to cause the two-dimensional aggregation and ordering of small colloidal particles observed in many experiments. The lateral capillary force between similar bodies is attractive, whereas between dissimilar bodies it is repulsive.

Energy and force approaches, which are alternative but equivalent, can be used for the theoretical description of the lateral capillary interactions. Both approaches require the Laplace equation of capillarity to be solved and the meniscus profile around the particles to be determined. The energy approach accounts for contributions due to the increase of the meniscus area, gravitational energy and/or energy of wetting. The second approach is based on calculating the net force exerted on the particle, which can originate from the hydrostatic pressure and interfacial tension. For small perturbations, the superposition approximation can be used to derive an asymptotic formula for the capillary forces, which has been found to agree well with the experiment. In all considered configurations of particles and interfaces the lateral capillary interaction originates from the overlap of interfacial deformations and is subject to a unified theoretical treatment, despite the fact that the characteristic particle size can vary from 1 cm down to 1 nm. (Protein molecules of nanometer size can be treated as "particles" insofar as they are considerably larger than the solvent (water) molecules.)

7.1. PHYSICAL ORIGIN OF THE LATERAL CAPILLARY FORCES

7.1.1. TYPES OF CAPILLARY FORCES AND RELATED STUDIES

The experience from experiment and practice shows that particles floating on a fluid interface attract each other and form clusters. Such effects are observed and utilized in some extraction and separation flotation processes [1,2]. Nicolson [3] developed an approximate theory of these lateral capillary forces taking into consideration the deformation of the interface due to the particle weight and buoyancy force. The shape of the surface perturbations created by floating particles has been studied by Hinsch [4] by means of a holographic method. Allain and Jouher [5], and in other experiment Allain and Cloitre [6], have studied the aggregation of spherical particles floating at the surface of water. Derjaguin and Starov [7] calculated theoretically the capillary force between two parallel vertical plates, or between two inclined plates, which are partially immersed in a liquid.

Additional interest in the capillary forces has been provoked by the fact that small colloidal particles and protein macromolecules confined in liquid films also exhibit attraction and do form clusters and larger ordered domains (2-dimensional arrays) [8-13]. The weight of such tiny particles is too small to create any substantial surface deformation. In spite of that, they also produce interfacial deformations because of the confinement in the liquid film combined with the effect of wettability of the particle surfaces. The wettability is related to the thermodynamic requirement that the interface must meet the particle surface at a given angle – the contact angle. The overlap of such wetting-driven deformations also gives rise to a lateral capillary force [14].

As already mentioned, the origin of the lateral capillary forces is the *deformation* of the liquid surface, which is supposed to be flat in the absence of particles. The larger the interfacial deformation created by the particles, the stronger the capillary interaction between them. Two similar particles floating on a liquid interface attract each other [3,15-17] - see Fig. 7.1a. This attraction appears because the liquid meniscus deforms in such a way that the gravitational potential energy of the two particles decreases when they approach each other. One sees that the origin of this force is the *particle weight* (including the Archimedes buoyancy force).

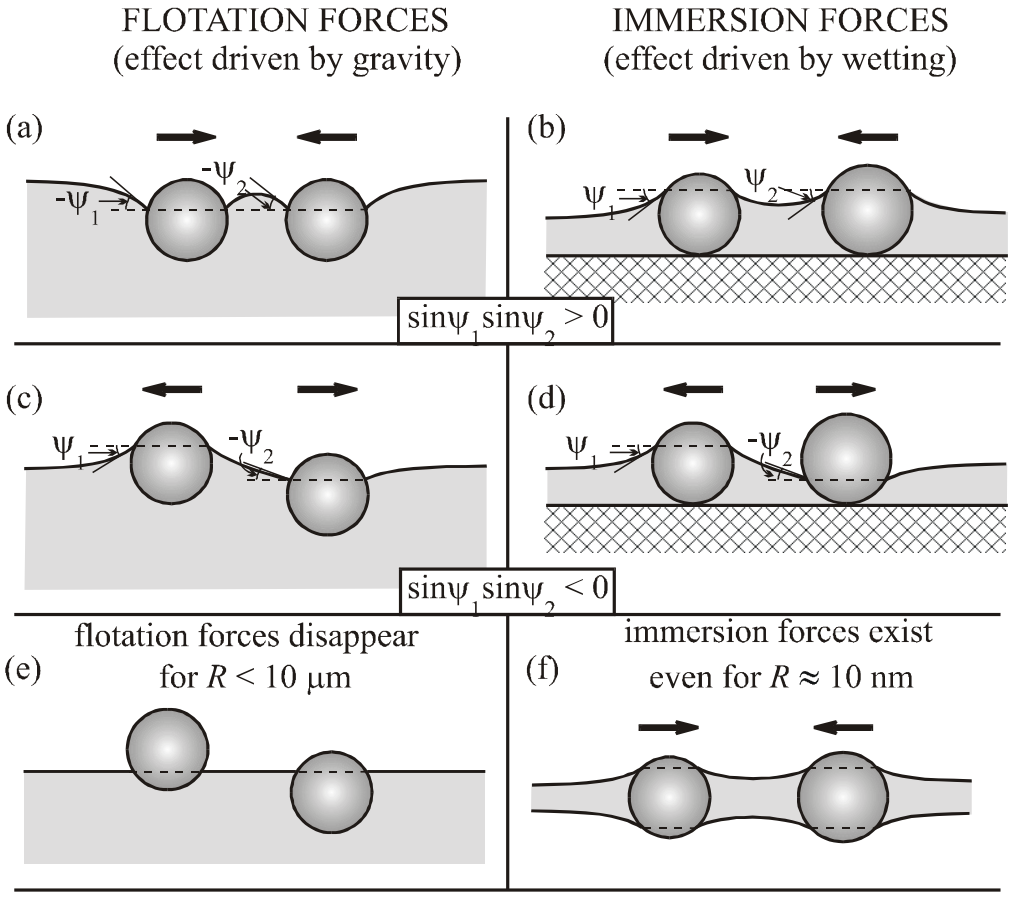

Fig. 7.1. Capillary forces of flotation (a,c,e) and immersion (b,d,f) type: (a) attraction between two similar floating particles; (b) attraction between two similar particles immersed in a liquid film on a substrate; (c) repulsion between a light and a heavy floating particle; (d) repulsion between a hydrophilic and a hydrophobic particle; (e) small floating particles do not deform the interface and do not interact; (f) small particles confined within a liquid film experience capillary interaction because they deform the film surfaces due to the effects of wetting [21].

Fig. 7.1b illustrates the other case in which force of capillary attraction appears: the particles (instead of being freely floating) are partially immersed (confined) into a liquid layer [14, 18-21]. The deformation of the liquid surface in this case is related to the *wetting properties* of the particle surface, i.e. to the position of the contact line and the magnitude of the contact angle, rather than to gravity.

To distinguish between the lateral forces in the case of floating particles and in the case of particles immersed in a liquid film, the former are called capillary *flotation* forces and the latter – capillary *immersion* forces [20,21]. These two kinds of force exhibit similar dependence on

the interparticle separation but very different dependencies on the particle radius and the surface tension of the liquid. The flotation and immersion forces can be both attractive (Fig. 7.1a and 7.1b) and repulsive (Fig. 7.1c and 7.1d). This is determined by the signs of the meniscus slope angles ψ_1 and ψ_2 at the two contact lines: the capillary force is attractive when $\sin\psi_1 \sin\psi_2 > 0$ and repulsive when $\sin\psi_1 \sin\psi_2 < 0$. In the case of flotation forces $\psi > 0$ for *light* particles (including bubbles) and $\psi < 0$ for *heavy* particles. In the case of immersion forces between particles protruding from an aqueous layer $\psi > 0$ for *hydrophilic* particles and $\psi < 0$ for *hydrophobic* particles. When $\psi = 0$ there is no meniscus deformation and, hence, there is no capillary interaction between the particles. This can happen when the weight of the particles is too small to create a significant surface deformation, Fig. 7.1e. The immersion force appears not only between particles in wetting films (Fig. 7.1b,d), but also in symmetric fluid films (Fig. 7.1f). Capillary immersion forces appear also between partially immersed bodies like vertical plates, vertical cylinders (rods), etc.

Nicolson [3] derived an approximated analytical expression for the capillary force between two floating bubbles. Calculations about the capillary force per unit length of two infinite parallel horizontal floating cylinders were carried out by Gifford and Scriven [15] and by Fortes [16]. In this simplest configuration the meniscus has a translational symmetry and the Laplace equation, describing the interfacial profile, acquires a relatively simple form in Cartesian coordinates [7,15,16]. Chan et al. [17] derived analytical expressions for floating horizontal cylinders and spheres using the Nicolson's superposition approximation and confirmed the validity of this approximation by a comparison with the exact numerical results for cylinders obtained by Gifford and Scriven [15].

The aforementioned studies [3,15-17] deal with floating particles, i.e. with flotation forces driven by the particle weight. For the first time the capillary forces between two vertical cylinders and between two spheres partially immersed in a liquid layer have been theoretically studied in Ref. [14]. A general expression for the interaction energy has been used [14], which includes contributions from the energy of particle wetting, the gravitational energy and the energy of increase of the meniscus area due to the deformation caused by the particles; this expression is valid for both floating and confined particles. Expressions and numerical results

for the energy and force of interaction have been obtained for the case of small slope of the deformed meniscus; this case has a physical and practical importance because it corresponds to the usual experimental situation with small particles. The theory has been extended also to particles entrapped in *thin* films, for which the disjoining pressure effect, rather than gravity, keeps the non-deformed surface planar [14].

A new moment in Ref. [14] is the analytical approach to solving the Laplace equation: instead of using the approximation about a mere superposition of the known axisymmetric profiles around two separate particles, the linearized Laplace equation has been solved directly in bipolar coordinates. Thus one can impose the correct boundary conditions (constancy of the contact angle in agreement with the Young equation) at the particle contact lines. Thus a more rigorous theoretical description of the force at small interparticle separations is achieved, which is not accessible to the superposition approximation.

Solutions for the meniscus profile in bipolar coordinates have been obtained in Ref. [18] for other configurations: vertical cylinder - vertical wall, and particle - vertical wall. A different, *force* approach to the calculation of the lateral capillary interactions has been applied to obtain both analytical and numerical results. It has been established that the force exerted on the particle and the wall have equal magnitudes and opposite signs, as required by the third Newton's law; this is a check of the validity of the derived analytical expressions, which are subject to some approximations (small particle, small meniscus slope).

The theory developed in Refs. [14] and [18] was further extended in Ref. [19] in the following two aspects. First, the energy approach and the force approach have been simultaneously applied to the *same* object (vertical cylinders and particles in a liquid film). The two approaches were found to give *numerically* coinciding results, although their equivalence had not been proven analytically there. Second, an analytical solution of Laplace equation in bipolar coordinates was obtained for the case of two *dissimilar* particles: vertical cylinders and/or spheres confined in a film. Attractive and repulsive capillary forces were obtained depending on the sings of the meniscus slopes at the contact lines of the two particles [19].

The theory of capillary forces between small *floating* particles of different size was extended in Ref. [20] on the basis of the results for the meniscus profile from Ref. [19]. The energy

approach was applied to calculate the capillary interaction. Appropriate analytical expressions have been derived and numerical results for various configurations were obtained. The superposition approximation of Nicolson [3] was derived as an asymptotic case of the general expression for the interaction free energy, and thus the validity of this approximation was analytically proven. It was noticed that in a wide range of distances the capillary forces obey a power law, which resembles the Coulomb's law of electricity. Following this analogy "capillary charges" of the particles have been introduced.

The physical nature and the magnitude of the lateral capillary forces between floating and confined particles have been compared in Ref. [20] and the differences between them have been explicitly analyzed. It has been established that the energy of capillary interaction between floating particles becomes negligible (smaller than the thermal energy kT) for particles smaller than 5–10 μm. On the other hand, when particles of the same size are partially immersed into a liquid film (instead of being freely floating), the energy of capillary interaction is much larger, and it can be much greater than kT even for particles of nanometer size. This analysis has been extended in Ref. [21] where the capillary forces in other configurations have been described theoretically; these are (i) two particles in a symmetric liquid film with account for the disjoining pressure effect, and (ii) two particles of fixed contact lines (rather than fixed contact angles). It has been established that the interaction at fixed contact angle is stronger than that at fixed contact line. Using the apparatus of the variational calculus the equivalence of the energy and force approaches to the capillary interactions has been analytically proven in Ref. [21] for the case of two vertical semi-immersed cylinders.

As noticed Ref. [18], the meniscus between a vertical cylinder (or particle) and a wall has the same shape as the meniscus between two identical particles, each of them being the image of the other one with respect to the wall. For that reason the capillary interaction between the particle and the wall is the same as between the particle and its mirror image. In this respect there is analogy with the image forces in electrostatics. This idea has been applied and developed in Refs. [22] and [23], in which the capillary image forces between particles floating over an inclined meniscus in a vicinity of a wall have been theoretically and experimentally investigated.

In Ref. [24] the theory of capillary forces has been extended to describe the interaction between particles attached to a *spherical* interface, film or membrane. In contrast with the planar interface (or film) the spherical interface has a restricted area and "infinite" interparticle separations are not possible. These geometrical differences can affect the trend of the lateral capillary force between identical particles: for spherical film it can be sometimes non-monotonic: repulsive at long distances and attractive at short distances. On the other hand, in the case of planar geometry the capillary force between identical particles is always monotonic attraction. In Ref. [25] the theory of the lateral capillary forces was extended to describe the interaction between inclusions in phospholipid membranes; for that purpose a special mechanical model accounting for the elastic properties of the lipid bilayer was developed.

A general conclusion from all studies on capillary immersion forces is that they are strong enough to produce aggregation and ordering of micrometer and sub-micrometer particles [14,18-25]. This fact could explain numerous experimental evidences about the formation of two-dimensional particle arrays in liquid films [26–45] and phospholipid membranes [46-48].

The problem about the capillary interaction between horizontal floating cylinders was reexamined by Allain and Cloitre [49,50], who used the linear superposition approximation and alternatively, a more rigorous expressions for the free energy of the cylinders; they calculated the capillary force for both light and heavy cylinders (for both small and large Bond numbers).

It should be noted that the lateral capillary forces are distinct from the popular *capillary bridge forces*, which form contacts between particles in the soil, pastes, and which are operative in some experiments with the atomic force microscope (AFM) [51-56]. The capillary bridge forces act *normally* to the plane of the contact line on the particle surface, while the lateral capillary forces are directed (almost) *tangentially* to the plane of the contact line.

Theory about another kind of capillary force, which can be operative between *particles of irregular wetting perimeter* has been proposed by Lucassen [57]. The irregular contact line induces respective irregular deformations in the surrounding liquid surface, even if the weight of the particle is negligible. The overlap of the deformations around such two particles also gives rise to a lateral capillary force. For the time being only a single theoretical study, Ref. [57], of this kind of force is available.

The present chapter is devoted to the capillary *immersion* forces. First we derive an asymptotic expression for the immersion forces at not-too-small separations and consider the comparison of this expression with the experiment. Next we present an appropriate solution of Laplace equation in bipolar coordinates and obtain more general expressions for the capillary immersion forces using the energy and force approaches. The following configurations are described theoretically: two semi-immersed vertical cylinders, two spherical particles, vertical cylinder and sphere, vertical cylinder (or sphere) and vertical wall. The boundary conditions for fixed contact *angle* and fixed contact *line* are considered.

The next Chapter 8 is devoted to the lateral capillary forces between two floating particles and between a floating particle and a wall (capillary image forces); applications of the theory of flotation forces to the measurement of the surface drag coefficient of small particles and the surface shear viscosity of surfactant adsorption monolayers are described. Chapter 9 presents the theory of the lateral capillary forces between particles bound to a *spherical* interface or thin film. An extension of the theory of the lateral capillary forces to the interactions between inclusions (membrane proteins) in *lipid bilayers* (biomembranes) is considered in Chapter 10.

7.1.2. LINEARIZED LAPLACE EQUATION FOR SLIGHTLY DEFORMED LIQUID INTERFACES AND FILMS

Let $z = \zeta(x,y)$ be the equation of the deformed fluid interface. The interfacial shape obeys the Laplace equation of capillarity, see Eqs. (2.15)–(2.17):

$$\nabla_{\mathrm{II}} \cdot \left(\frac{\nabla_{\mathrm{II}} \zeta}{\sqrt{1 + \left| \nabla_{\mathrm{II}} \zeta \right|^2}} \right) = [P_{\mathrm{II}}(\zeta) - P_{\mathrm{I}}(\zeta)]/\sigma \tag{7.1}$$

$$\nabla_{\mathrm{II}} \equiv \mathbf{e}_x \frac{\partial}{\partial x} + \mathbf{e}_y \frac{\partial}{\partial y} \tag{7.2}$$

Here, as usual, ∇_{II} is the two-dimensional gradient operator in the plane xy. Note that Eq. (7.1) is expressed in a covariant form and can be specified for any type of curvilinear coordinates in the plane xy (not only Cartesian ones). The pressures P_{I} and P_{II} on the two sides of the interface can dependent on ζ because of the effects of hydrostatic pressure and disjoining pressure, see below.

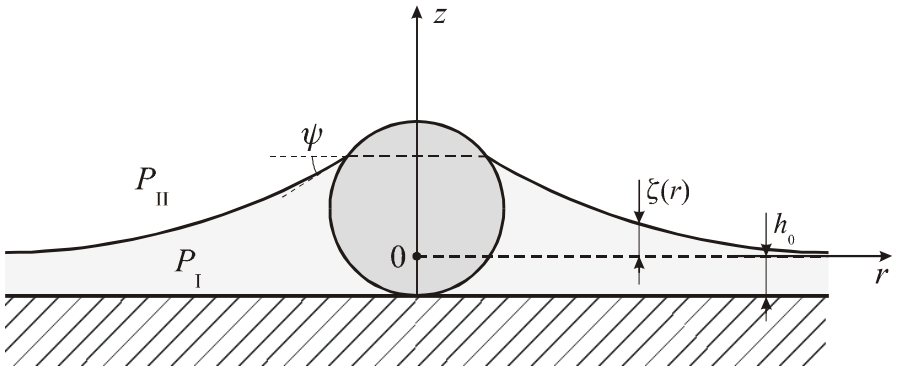

Fig. 7.2. Colloidal sphere partially immersed in a liquid layer on a substrate; $\zeta(r)$ describes the shape of the meniscus formed around the sphere; P_{I} and P_{II} are the pressures inside the liquid layer and in the upper fluid phase; h_0 is the thickness of the non-disturbed liquid layer; the latter is kept plane-parallel by the gravity, when the layer is thick, and by a repulsive disjoining pressure when the film is thin.

As an example, let us consider a spherical particle which is entrapped into a wetting liquid film, Fig. 7.2. The upper surface of the liquid film is planar far from the particle; this plane is chosen to be the level $z = 0$ of the coordinate system. The thickness of the plane-parallel liquid film far from the particle is h_0. The pressure inside and outside the film (in phases I and II) can be expressed in the form [58,59,21]:

$$P_{\mathrm{I}}(\zeta) = P_{\mathrm{I}}^{(0)} - \rho_{\mathrm{I}} g\zeta + \Pi(h_0+\zeta), \qquad P_{\mathrm{II}}(\zeta) = P_{\mathrm{II}}^{(0)} - \rho_{\mathrm{II}} g\zeta,, \qquad |\nabla_{\mathrm{II}}\zeta|^2 << 1 \qquad (7.3)$$

Here, as before, g is the acceleration due to gravity, ρ_{I} and ρ_{II} are the mass densities in phases I and II, $P_{\mathrm{I}}^{(0)}$ and $P_{\mathrm{II}}^{(0)}$ are the pressures in the respective phases at the level $z = 0$; Π is the disjoining pressure, which depends on the local thickness of the wetting film. The terms $\rho_{\mathrm{I}} g\zeta,$ and $\rho_{\mathrm{II}} g\zeta,$ express the hydrostatic pressure effect, which is predominant in thick films, i.e. for $h_0 >> 100$ nm, in which the disjoining pressure Π (the interaction between the two adjacent phases across the liquid film) becomes negligible. In fact, the gravity keeps the interface planar (horizontal) far from the particle when the film is *thick*. On the contrary, when the film is *thin*, the existence of a positive disjoining pressure (repulsion between the two film surfaces) keeps the film plane-parallel far from the particle, supposedly the substrate is planar. The condition for stable mechanical equilibrium of this film is

$$P_{\mathrm{II}}^{(0)} = P_{\mathrm{I}}^{(0)} + \Pi(h_0), \qquad \Pi' \equiv \left(\frac{\partial \Pi}{\partial h}\right)_{h=h_0} < 0 \tag{7.4}$$

see e.g. Ref. [60]. Expanding the disjoining pressure term in Eq. (7.3) in series one obtains

$$\Pi(h_0+\zeta) = \Pi(h_0) + \Pi' \zeta + \ldots \tag{7.5}$$

Usually the slope of the meniscus around particles, like that depicted in Fig. 7.2, is small enough and the approximation $|\nabla_{\mathrm{II}}\zeta|^2 << 1$ can be applied. Then combining Eqs. (7.1)–(7.5) one obtains a linearized form of Laplace equation [14]:

$$\nabla_{\mathrm{II}}^2 \zeta = q^2 \zeta, \qquad q^2 \equiv \frac{\Delta\rho g}{\sigma} + \frac{-\Pi'}{\sigma} \qquad (\Delta\rho \equiv \rho_{\mathrm{I}} - \rho_{\mathrm{II}},\ |\nabla_{\mathrm{II}}\zeta|^2 << 1) \tag{7.6}$$

Note that $\Pi' < 0$. The disjoining pressure effect is negligible when the film is thick enough to have $-\Pi'(h_0) << \Delta\rho g$. In the latter case the upper film surface behaves as a single interface (it does not "feel" the lower film surface). The quantity q^{-1} is a characteristic capillary length, which determines the range of action of the lateral capillary forces. In thick films Π' is negligible and q^{-1} is of the order of millimeters, e.g. q^{-1} = 2.7 mm for water-air interface. However, in thin films Π' is predominant and q^{-1} can be of the order of 10–100 nm, see Ref. [21]. In other words, the asymptotic expressions for q^2 are:

$$\begin{aligned} q^2 &= \Delta\rho g / \sigma \qquad (\text{in thick film}) \\ q^2 &= -\Pi' / \sigma \qquad (\text{in thin films}) \end{aligned} \tag{7.7}$$

7.1.3. IMMERSION FORCE: THEORETICAL EXPRESSION IN SUPERPOSITION APPROXIMATION

Following Ref. [64] let us consider a couple of vertical cylinders, each of them being immersed partially in phase I, and partially in phase II. For each of these cylinders in isolation (Fig. 7.3) the shape of the surrounding capillary meniscus can be obtained by solving Eq. (7.6). The latter equation, written in cylindrical coordinates, reduces to the modified Bessel equation, whose solution (for small meniscus slope) has the form

$$\zeta_k(r) = r_k \sin\psi_k \, \mathrm{K}_0(qr) = Q_k \, \mathrm{K}_0(qr), \qquad (k = 1,2) \tag{7.8}$$

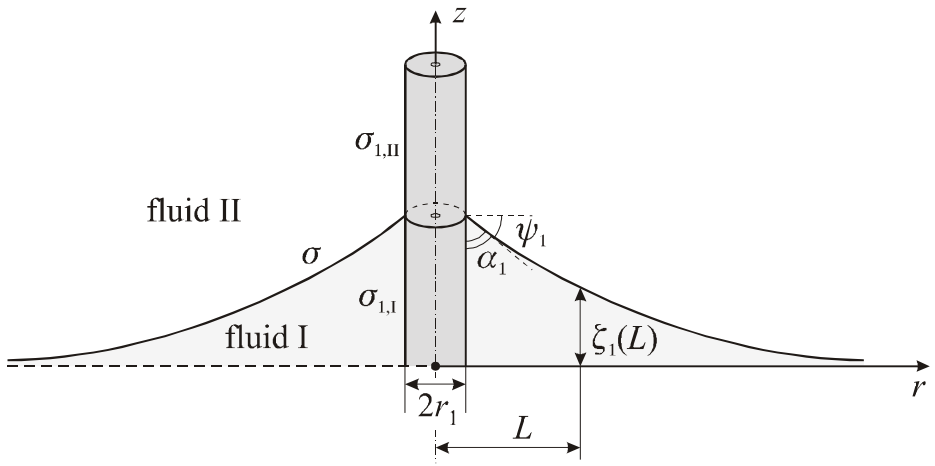

Fig. 7.3. A vertical cylinder (rod) of radius r_1 creates a convex meniscus on an otherwise horizontal fluid interface of tension σ; the boundaries of the cylinder with the phases I and II have solid-fluid surface tensions $\sigma_{1,I}$ and $\sigma_{1,II}$; α_1 is the three-phase contact angle; ψ_1 is the meniscus slope at the particle contact line.

see Eq. (2.43), where r_k is the contact line radius and ψ_k is the meniscus slope angle at the contact line, and is the so called "capillary charge" [20,21]; K_0 is the Macdonald function of

$$Q_k \equiv r_k \sin\psi_k \qquad (k = 1,2) \tag{7.9}$$

zero order, see Refs. [61-63]. The contact angle α_k at the three phase contact line of the k-th cylinder ($k = 1,2$) obeys the Young equation:

$$\sigma_{k,II} - \sigma_{k,I} = \sigma\cos\alpha_k = \sigma\sin\psi_k = \sigma Q_k/r_k \qquad (k = 1,2) \tag{7.10}$$

cf. Fig. 7.3 and Eq. (2.2). Here $\sigma_{k,I}$ and $\sigma_{k,II}$ are the superficial tensions of fluids I and II, respectively, with solid 'k', see Section 2.3.1. The two cylinders are assumed immobile in vertical direction.

Let us assume that cylinder 1 is fixed at the z-axis (Fig. 7.3) and let us consider a process in which the vertical cylinder 2 is moved in horizontal direction from infinity to some finite distance L ($L >> r_1,r_2$). At a distance L the level of the liquid meniscus created by cylinder 1 is $\zeta_1(L)$, see Fig. 7.3, and consequently, the elevation of the liquid around cylinder 2 rises with $\zeta_1(L)$. Thus the surface area of cylinder 2 wet by phase I increases, whereas the area wet by phase II decreases. As a result, the energy of wetting of cylinder 2 will change with [64]

$$\Delta W_w \approx -2\pi r_2 \zeta_1(L)\,(\sigma_{2,\mathrm{II}} - \sigma_{2,\mathrm{I}}) = -2\pi\sigma Q_1 Q_2 \mathrm{K}_0(qL) \tag{7.11}$$

where at the last step Eqs. (7.8)–(7.10) have been used. Finally, identifying the capillary force with the derivative of the wetting energy, $F = -d\Delta W_w/dL$, we differentiate Eq. (7.11) using the identity [61,62]

$$\mathrm{dK}_0(x)/\mathrm{d}x \equiv -\mathrm{K}_1(x) \tag{7.12}$$

and thus we obtain an (approximate) expression for the capillary immersion force [21,64]:

$$F = -2\pi\sigma Q_1 Q_2 q \mathrm{K}_1(qL), \qquad r_k << L \tag{7.13}$$

Similar approximate expression for the flotation capillary force has been obtained long ago by Nicolson [3]; see also Refs. [17] and [20]. A more rigorous expression for F is given by Eq. (7.86) below. The above derivation of Eq. (7.13) makes use of the approximations $r_i << L$, $|\nabla_{\mathrm{II}}\zeta|^2 << 1$. In particular, we have implicitly made use of the assumption, that for $L >> r_i$ the elevation of the liquid at cylinder 2 is equal to the superposition of the elevation at the isolated cylinder 2 plus the elevation $\zeta_1(L)$ created by cylinder 1 at a distance L. The latter assumption is known as the superposition approximation; it can be obtained as an asymptotic case of the more rigorous solution, see Eq. (7.89) below. In the case of spherical particles the variation in the position of the contact line on the particle surface is accompanied with a variation of the contact line radii, r_1 and r_2, and of the slope angles ψ_1 and ψ_2 ; these effects are taken into account in Refs. [14,18-20,24], see Section 7.3.2 for details.

In spite of being approximate, the derivation of Eq. (7.13), clearly demonstrates the physical origin of the immersion force: the latter is (approximately) equal to the derivative of the *wetting* energy W_w, see Eq. (7.11); similarly one can obtain (Section 8.1.1) that the flotation force can be approximated with the derivative of the *gravitational* energy W_g of a floating particle, which as a final result gives again Eq. (7.13). Using the identity $\mathrm{K}_1(x) \approx 1/x$ for $x << 1$ [61,62,65], one derives the asymptotic form of Eq. (7.13) for $qL << 1$ ($q^{-1} = 2.7$ mm for water),

$$F = -2\pi\sigma \frac{Q_1 Q_2}{L} \qquad r_k << L << q^{-1}, \tag{7.14}$$

which looks like a two-dimensional analogue of Coulomb's law of electrostatics. The latter fact explains the name "capillary charge" of Q_1 or Q_2 [20,21].

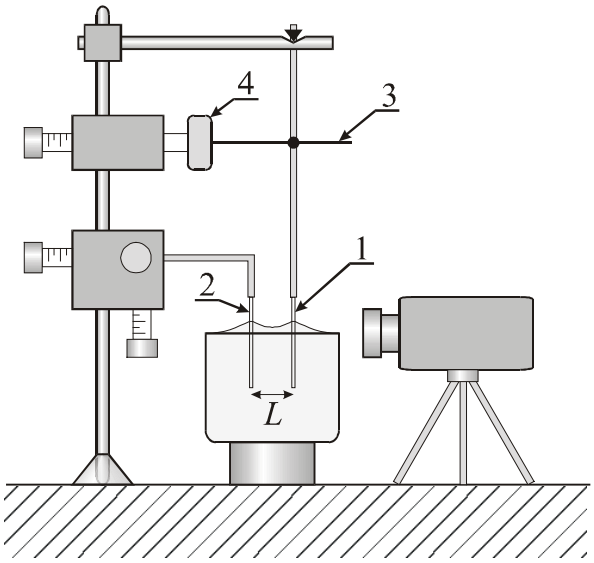

Fig. 7.4. Sketch of the experimental set up used in Ref. [67] to measure the capillary immersion force between two vertical cylinders, '1' and '2'; '3' is a glass needle, which transfers the horizontal force exerted on cylinder '1' to a piezo-resistive sensor '4'. Thus the force, converted into electric signal, is measured as a function of the distance L.

7.1.4. MEASUREMENTS OF CAPILLARY IMMERSION FORCES

Measurement of lateral capillary force (of the immersion type) has been carried out by Camoin et al. [66] with millimeter-sized polystyrene spheres attached to the tip of rod-like holders. By means of a sensitive electro-mechanical balance it has been established that the force is attractive and decays (approximately) exponentially, which corresponds to the long-distance asymptotics of Eq. (7.13), see e.g. Refs. [61, 65]:

$$F \approx -\pi\sigma Q_1 Q_2 \left(\frac{2\pi q}{L}\right)^{1/2} \exp(-qL)\left[1 + O\left(\frac{1}{qL}\right)\right] \qquad (qL \geq 2) \qquad (7.15)$$

A detailed comparison of the experimental results from Ref. [62] with the theory is not possible, because data for the surface tension, contact angle and the contact line radius are not given in that paper.

Capillary immersion forces between two vertical cylinders, and between a vertical cylinder and a wall, were measured by means of a piezo-transduser balance [67], see Fig. 7.4. One of the cylinders ('1' in Fig. 7.4) is connected by a thin glass needle to a piezoresistive sensor; thus

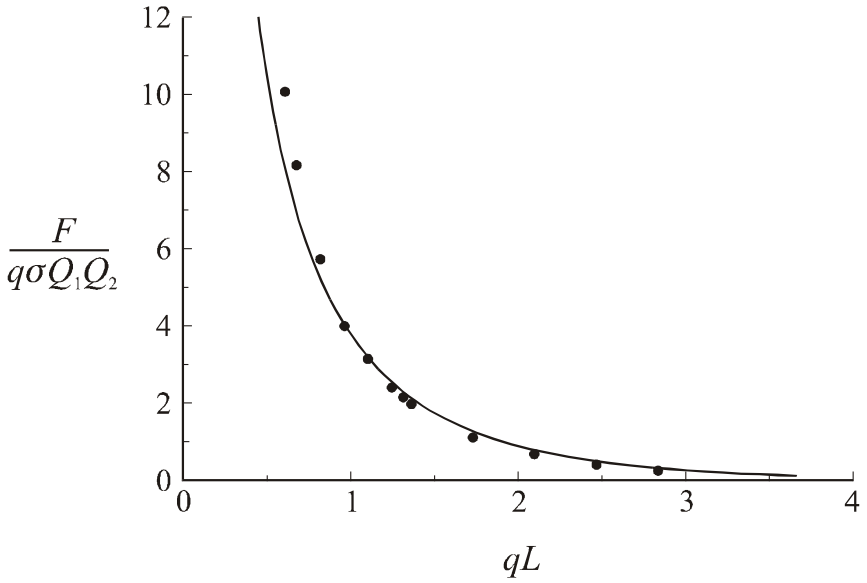

Fig. 7.5. Force F of capillary attraction between two hydrophilic vertical cylinders measured in Ref. [67] by means of the piezo-transducer balance sketched in Fig. 7.4; F is plotted vs. the distance L between the axes of the cylinders; the parameters values are q^{-1} = 2.72 mm, σ = 72.4 mN/m, Q_1 = 0.370 mm, Q_2 = 0.315 mm. The solid line is calculated by means of Eq. (7.13); no adjustable parameters.

the sensor can detect the pressure caused by the needle, which is in fact the horizontal component of the force exerted on the vertical cylinder 1. The other cylinder 2 can be moved during the experiment in order to change the distance L between the bodies. Figure 7.5 presents the dimensionless attractive capillary force $F/(q\sigma Q_1 Q_2)$ vs. the dimensionless distance qL measured in Ref. [67]. The liquid is pure water, σ = 72.4 mN/m, q^{-1} = 2.72 mm; the two cylinders are hydrophilic, so $\psi_1 = \psi_2 = 90°$; the radii of the cylinders are r_1 = 370 μm and r_2 = 315 μm.

The solid curve in Fig. 7.5 is drawn by means of Eq. (7.13) without using any adjustable parameters. One sees that Eq. (7.13) agrees well with the experiment except in the region of small distances, where the asymptotic formula (7.13), derived under the assumptions for small meniscus slope and long distances, is no longer valid.

The experimental data in Fig. 7.5 correspond to attraction between two *similar* (hydrophilic) rods. On the other hand, repulsive capillary force have been detected between two *dissimilar*

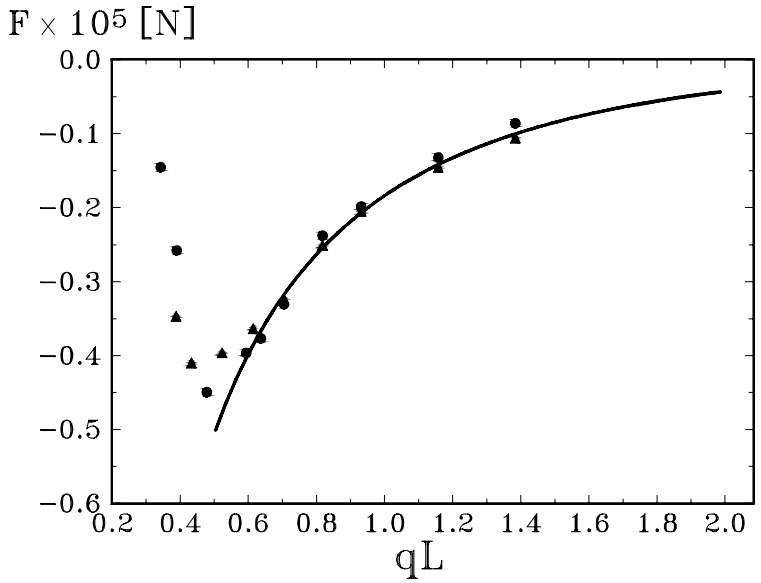

Fig. 7.6. Force F of capillary repulsion between hydrophilic ($\alpha_1 = 0°$, $r_1 = 370$ μm) and hydrophobic ($\alpha_2 = 99°$, $r_2 = 315$ μm) vertical cylinders measured in Ref. [67] by means of the balance sketched in Fig. 7.4; F is plotted vs. the distance L between the axes of the cylinders; the parameters values are $q^{-1} = 2.72$ mm, $\sigma = 72.4$ mN/m. The circles and triangles are results from two separate runs. The solid line is calculated by means of Eq. (7.13); no adjustable parameters.

rods, a hydrophilic and a hydrophobic one, see Fig. 7.6. At long distances the experimental data agree very well with Eq. (7.13): see the solid curve in Fig. 7.6, which is drawn without using any adjustable parameter. For short distances the data do not comply with Eq. (7.13), which is a manifestation of non-linear effects.

Systematic measurements of capillary immersion force between partially immersed bodies of various shape (two vertical cylinders, cylinder and sphere, two spheres, sphere and vertical wall) were carried out in Refs. [68-70] by means of a torsion micro-balance, see Fig. 7.7. The latter in principle somewhat resembles the balance used by H. Cavendish to determine the gravitational constant in 1798 [71], but is much smaller. The interaction force for two couples of vertical cylinders and/or spheres (Fig. 7.7) was measured by counterbalancing the moment created by the two couples of forces with the torsion moment of a fine platinum wire, whose diameter was 10 μm and 25 μm in different experiments. The angle of torsion, φ, was measured by reflection of a laser beam from a mirror attached to the anchor of the balance, see Fig. 7.7. Figure 7.8 shows data from Ref. [68] for the capillary force between two identical

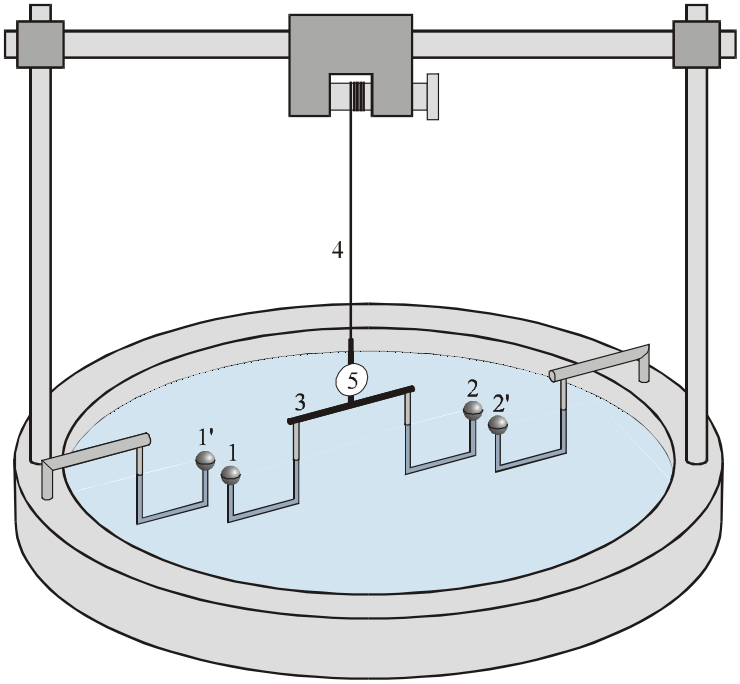

Fig. 7.7. Sketch of a torsion balance, used in Refs. [68-70] to measure the capillary attraction between two pairs of small, partially immersed, glass spheres (1-1' and 2-2') attached to holders. The immersed part of the holders is shown dashed. One of the particles in each pair (these are particles 1 and 2) is connected to the central anchor 3, which is suspended on a platinum wire 4; the angle of torsion is measured by reflection of a light beam from the mirror 5.

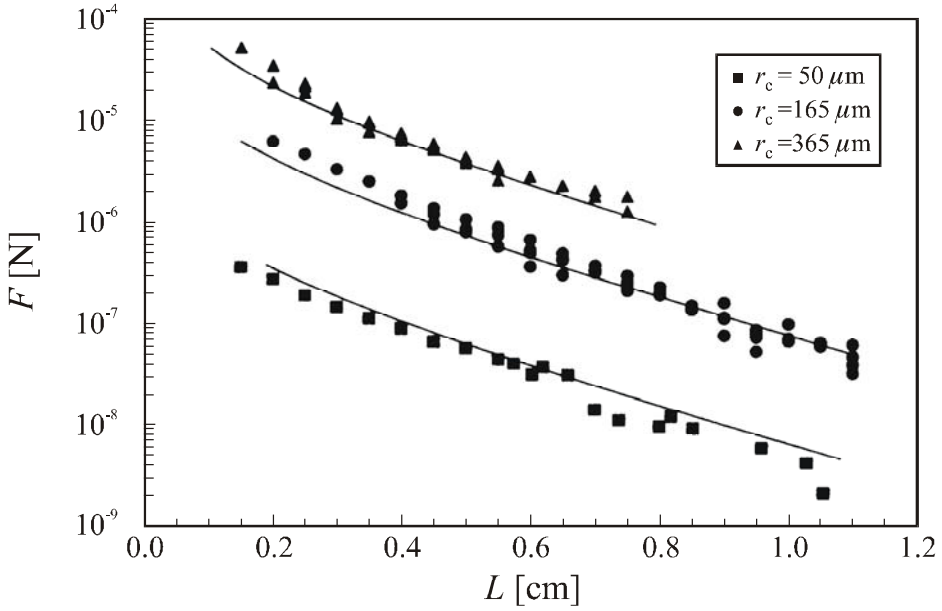

Fig. 7.8. Plot of the force of capillary attraction F vs. the distance L between the axes of two identical vertical cylinders of radius r_c. The force is measured in Refs. [68] by means of the torsion balance shown in Fig. 7.7; the three curves correspond to r_c = 50, 165 and 365 μm. The solid lines are drawn by means of Eq. (7.13); no adjustable parameters.

vertical cylinders for $r_1 = r_2 = 50$, 165 and 365 μm; the solid lines in Fig. 7.8 are calculated by means of Eq. (7.13) without using any adjustable parameter. It is seen that the theory and experiment agree well in the range of validity of the theoretical expressions. At shorter distances between the two interacting bodies, at which the linearized theory is not accurate, deviations from Eq. (7.13) are experimentally detected [69], as it could be expected.

7.1.5. ENERGY AND FORCE APPROACHES TO THE LATERAL CAPILLARY INTERACTIONS

The *energy approach* to the lateral capillary interactions (both immersion and flotation) is based on an expression for the grand thermodynamic potential of a system of N particles attached to the interface between phases 1 and 2, which can be written in the form [14,20,21]:

$$\Omega(\mathbf{r}_1,...,\mathbf{r}_N) = W_g + W_w + W_m + \text{const.} \tag{7.16}$$

$$W_g = \sum_{k=1}^{N} m_k g Z_k^{(c)} - \sum_{Y=\mathrm{I,II}} \int_{V_Y} P_Y dV \tag{7.17}$$

$$W_w = \sum_{k=1}^{N} \sum_{Y=\mathrm{I,II}} \sigma_{kY} A_{kY}, \qquad W_m = \sigma \Delta A, \tag{7.18}$$

where $\mathbf{r}_1$, $\mathbf{r}_2$,...,$\mathbf{r}_N$ are the position vectors of the particle mass centers and m_k (k = 1,2,...,N) are the masses of the particles, $Z_i^{(c)}$ is the projection of $\mathbf{r}_k$ along the vertical, P_Y and V_Y (Y = I,II) are pressure and volume of the fluid phases I and II; σ is the surface tension of the interface (the meniscus) between fluid phases I and II; ΔA is the difference between the area of this meniscus and the area of its projection on the plane xy (ΔA is finite even if the meniscus has infinite area, i.e. levels off to a plane at infinity); A_{kY} and σ_{kY} are area and the surface free energy density of the boundary between particle *'k'* and phase *'Y'*; the additive constant in Eq. (7.16) does not depend on $\mathbf{r}_1$, $\mathbf{r}_2$,...,$\mathbf{r}_N$. W_g, W_w and W_m are respectively the gravitational, wetting and meniscus contribution to the grand potential Ω. Then the lateral capillary force between particles 1 and 2 is determined by differentiation:

$$F^{(12)} = -\frac{\partial \Omega}{\partial r_{12}}, \qquad r_{12} = |\mathbf{r}_1 - \mathbf{r}_2| \tag{7.19}$$

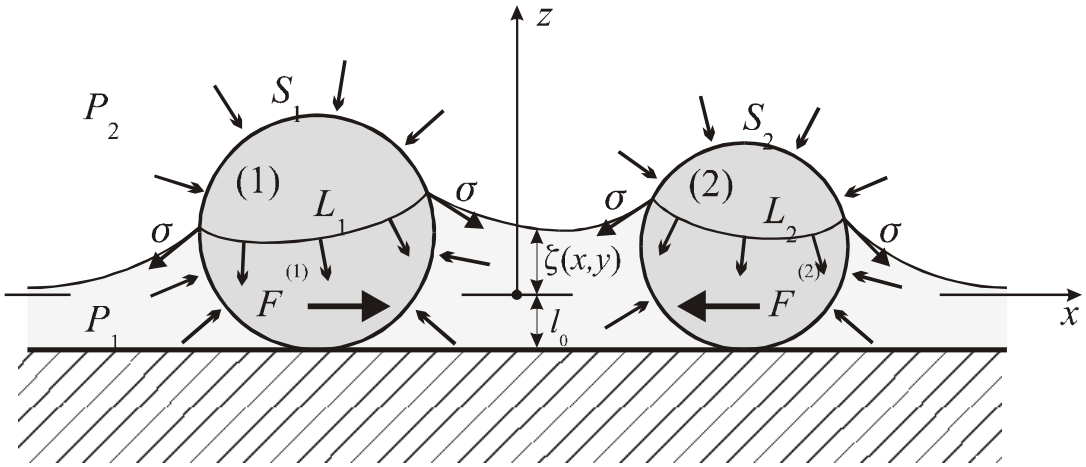

Fig. 7.9. Illustration of the origin of capillary force between two spheres partially immersed in a liquid film: The net horizontal force $\mathbf{F}^{(1)}$ exerted on particle 1 is a sum of the surface tension vector $\boldsymbol{\sigma}$ integrated along the contact line L_1 and of the pressure distribution integrated throughout the particle surface S_1 (the same for particle 2), see Eqs. (7.21)–(7.23).

When the distance between two particles varies, the shape of the meniscus between phases I and II (and consequently W_m) alters; during the same variation the areas of the particle surfaces wet by phases I and II also vary, which leads to a change in W_w; last but not least, the change in the meniscus shape is accompanied by changes in the positions of the mass centers of particles and fluid phases, which gives rise to a variation in their gravitational energy accounted for by W_g. Equations (7.16)–(7.19) are applicable also to thin films; one should take into account the fact that in such a case the meniscus surface tension depends on the local thickness of the film, $\sigma = \sigma(\zeta)$, so that [21,72]

$$\frac{d\sigma}{d\zeta} = -\left(1 + \left|\nabla_{II}\zeta\right|^2\right)^{-1/2}\Pi \qquad \text{(thin films)} \qquad (7.20)$$

where, as usual, Π is the disjoining pressure. In other words, the disjoining pressure effect is "hidden" in the meniscus energy term, W_m, in Eq. (7.16).

The explicit form of Eqs. (7.14) and (7.15), and the relative importance of W_g, W_w and W_m, depend on the specific configuration of the system. For example, in the case of flotation force Ω is dominated by W_g, whereas in the case of immersion force Ω is dominated by W_w. This leads to different expressions for Ω corresponding to different physical configurations.

In the *force* approach, which is different but equivalent to the above *energy* approach, the lateral capillary force exerted on each of the interacting particles is calculated by integrating the meniscus interfacial tension $\boldsymbol{\sigma}$ along the contact line and the hydrostatic pressure P throughout the particle surface [18-21]:

$$\mathbf{F}^{(k)} = \mathbf{F}^{(k\sigma)} + \mathbf{F}^{(k\mathrm{p})}, \qquad k = 1,2,..., \tag{7.21}$$

where the contribution of interfacial tension is

$$\mathbf{F}^{(k\sigma)} \equiv \mathbf{U}_{\mathrm{II}} \cdot \oint_{L_k} dl\, \mathbf{m}\sigma \qquad k = 1,2,..., \tag{7.22}$$

and the contribution of the hydrostatic pressure is

$$\mathbf{F}^{(k\mathrm{p})} \equiv \mathbf{U}_{\mathrm{II}} \cdot \oint_{S_k} ds(-\mathbf{n}\, P) \qquad k = 1,2,.... \tag{7.23}$$

Here $\mathbf{U}_{\mathrm{II}}$ is the unit operator (tensor) of the horizontal plane xy; in Eqs. (7.22) and (7.23) this operator projects the respective vectorial integrals onto the xy-plane; L_k denotes the three phase contact line on the particle surface (Fig. 7.9) and dl is a linear element; the vector of surface tension $\underline{\boldsymbol{\sigma}} = \mathbf{m}\sigma$ exerted per unit length of the contact line on the particle surface, is simultaneously normal to the contact line and tangential to the meniscus, and has magnitude equal to the surface tension σ; $\mathbf{m}$ is a unit vector; S_k denotes the particle surface with outer unit running normal $\mathbf{n}$; ds is a scalar surface element; the vector '$-\mathbf{n}$' has the direction of the outer pressure exerted on the surface of each particle. In Refs. [18,19,21] it has been proven, that the integral expressions (7.21)–(7.23) are compatible with the Newton's third law, i.e. $\mathbf{F}^{(1)} = -\mathbf{F}^{(2)}$, as it must be.

Note that the interfacial bending moment can also contribute to the lateral capillary force, see Ref. [25] and Chapter 10 below, although this contribution is expected to be important only for interfaces and membranes of low tension σ.

As an example, let us consider two particles entrapped in a liquid film on a substrate, see Fig. 7.9. If the contact lines L_1 and L_2 were horizontal, the integrals in Eqs. (7.22) and (7.23) would be equal to zero because of the symmetry of the force distributions. However, due to the overlap of the interfacial perturbations created by each particle, the contact lines are slightly

inclined, which is enough to break the symmetry of the force distribution and to give rise to a non-zero net (integral) force exerted on each of the two particles, $F^{(1)}$ and $F^{(2)}$ in Fig. 7.9.

The existence of inclination of the contact line can be clearly seen in Fig. 7.10, which represents three photographs of thin vertical hydrophobic glass rods partially immersed in water; the photographs have been taken Velev et al. [67] with the experimental set up sketched in Fig. 7.4. One sees that the contact line on an isolated rod is horizontal (Fig. 7.10a); when two such rods approach each other inclination of the contact line appears (Fig. 7.10b) and grows with the decrease of the distance between the rods (Fig. 7.10c).

Let us imagine now that the upper part of the rods shown in Fig. 7.10 is hydrophobic, whereas the lower part is hydrophilic. In such a case the three-phase contact line can stick to the horizontal boundary between the hydrophobic and hydrophilic regions and the contact line will remain immobile and horizontal (no inclination!) when the two rods approach each other.

Nevertheless, in such a case a lateral force of capillary attraction will also appear [21] because of the contact angle hysteresis: the meniscus slope varies along the circular contact line of each rod. The meniscus slope is the smallest in the zone between the two vertical cylinders (rods); then the integration in Eq. (7.22) yields again an attractive net force, see Ref. [21] and Section 7.3.4 for more details.

It is worth noting that for small particles, $r_1, r_2 << q^{-1}$, the contribution of the pressure to the capillary force is negligible,

$$|\mathbf{F}^{(k\mathrm{p})}| << |\mathbf{F}^{(k\sigma)}| \qquad \text{for } r_1, r_2 << q^{-1}, \tag{7.24}$$

see Refs. [19,20] and Section 7.4 below. As established by Allain and Cloitre [49], the pressure contribution can prevail for $\zeta(r_k) >> q^{-1}$ (k = 1,2), i.e. for large Bond numbers; however, this is not the case with colloidal particles, for which Eq. (7.24) is satisfied.

It is not obvious that the energy and force approaches, based on Eqs. (7.16)–(7.19) and (7.21)–(7.23), respectively, are equivalent. Numerical coincidence of the results provided by these two approaches has been established in Refs. [19,20]. Analytical proof of the equivalence of the two approaches has been given in Ref. [21] for the case of two vertical cylinders; Eqs. (7.21)–(7.23) are derived by a differentiation of Ω, see Eqs. (7.16) and (7.19).

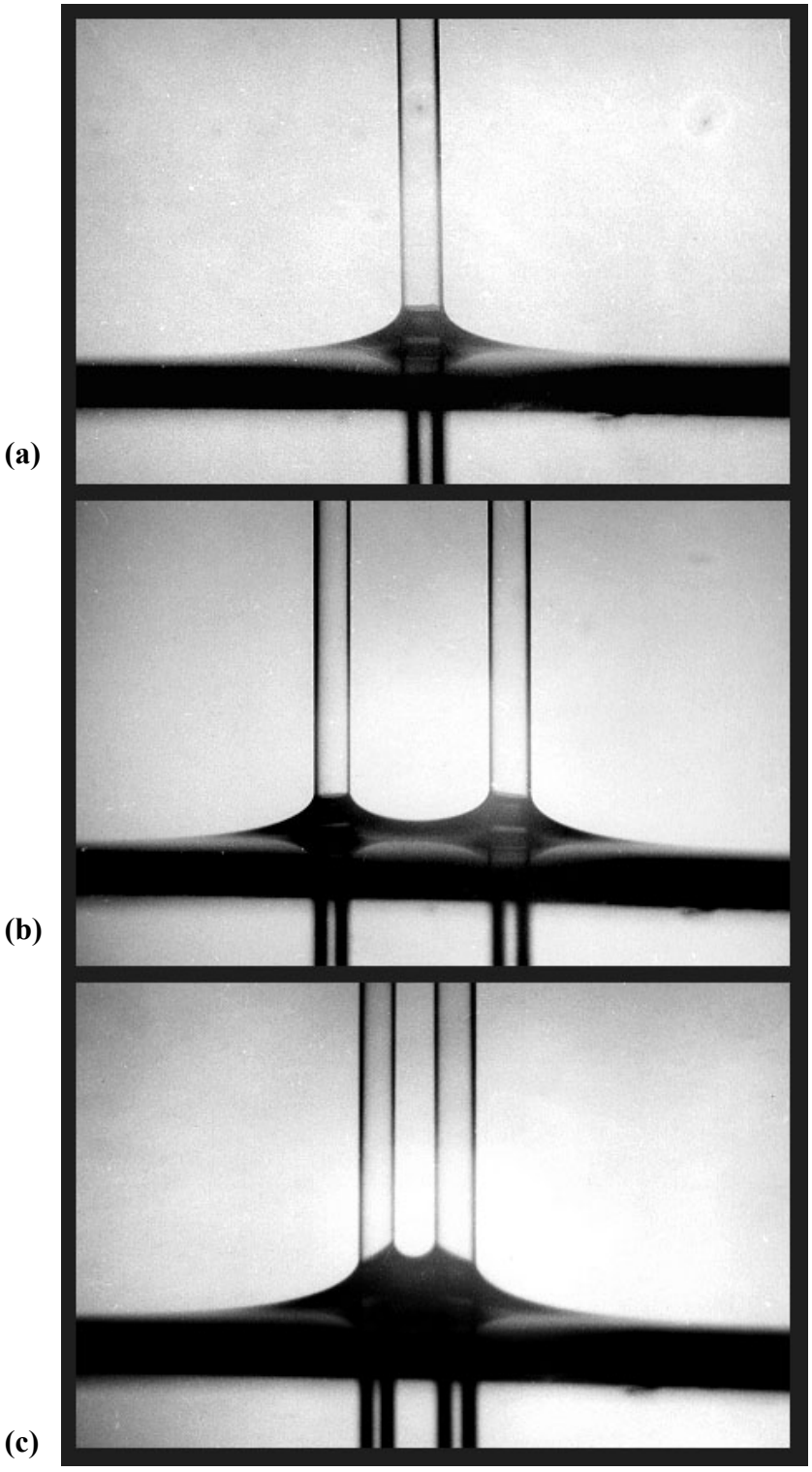

Fig. 7.10. Photographs, taken by Velev et al. [67], of two partially immersed vertical hydrophilic glass rods of radii r_1 = 315 μm and r_2 = 370 μm. Note that the inclination of the three-phase contact lines on the rods increases when the distance between them decreases.

7.2. SHAPE OF THE CAPILLARY MENISCUS AROUND TWO AXISYMMETRIC BODIES

7.2.1. SOLUTION OF THE LINEARIZED LAPLACE EQUATION IN BIPOLAR COORDINATES

When the Young equation holds and the three-phase contact angle is constant, the appearance of a small inclination of the contact line gives rise to the lateral capillary force, see Fig. 7.9. The simple superposition approximation is too rough to provide a quantitative estimate of this fine inclination. Indeed, the meniscus shape in superposition approximation does not satisfy the boundary condition for the constancy of the contact angle at the particle surface. A quantitative description can be obtained by solving the linearized Laplace equation, Eq. (7.6), in bipolar (bicylindrical) coordinates (τ, ω) in the plane xy, see e.g. Ref. [63]

$$x = \frac{a \sinh \tau}{\cosh \tau - \cos \omega}, \qquad y = \frac{a \sin \omega}{\cosh \tau - \cos \omega} \tag{7.25}$$

$$-\tau_1 \le \tau \le \tau_2 , \qquad -\pi \le \omega \le \pi \tag{7.26}$$

The elementary lengths along the τ- and σ-lines of the respective orthogonal curvilinear coordinate network are [63]

$$dl_\tau = \sqrt{g_{\tau\tau}}\, d\tau, \qquad dl_\omega = \sqrt{g_{\omega\omega}}\, d\omega, \qquad g_{\tau\tau} = g_{\omega\omega} = \frac{a^2}{(\cosh \tau - \cos \omega)^2} \tag{7.27}$$

where $g_{\tau\tau}$ and $g_{\omega\omega}$ are components of the metric tensor. In Fig. 7.11 the circumferences C_1 and C_2, of radii r_1 and r_2, represent the projections of the contact lines L_1 and L_2 on two interacting particles onto the plane xy (see e.g. Fig. 7.9). In the case of two vertical rods C_1 and C_2 will be exactly circumferences; in the case of two spheres (Fig. 7.9) the contours C_1 and C_2 will slightly deviate from the circular shape, but this deviation is small for small particles, that is for $(qr_k)^2 << 1$, and can be neglected [14]. The x-axis in Fig. 7.11 is chosen to pass through the centers of the two circumferences. The coordinate origin is determined in such a way that the tangents OA_1 and OA_2 to have equal lengths, a; in fact this is the geometrical meaning of parameter a in Eq. (7.25). From the two rectangular triangles in Fig. 7.11, OO_1A_1 and OO_2A_2, one obtains

$$s_k^2 - a^2 = r_k^2, \qquad (k = 1,2). \tag{7.28}$$

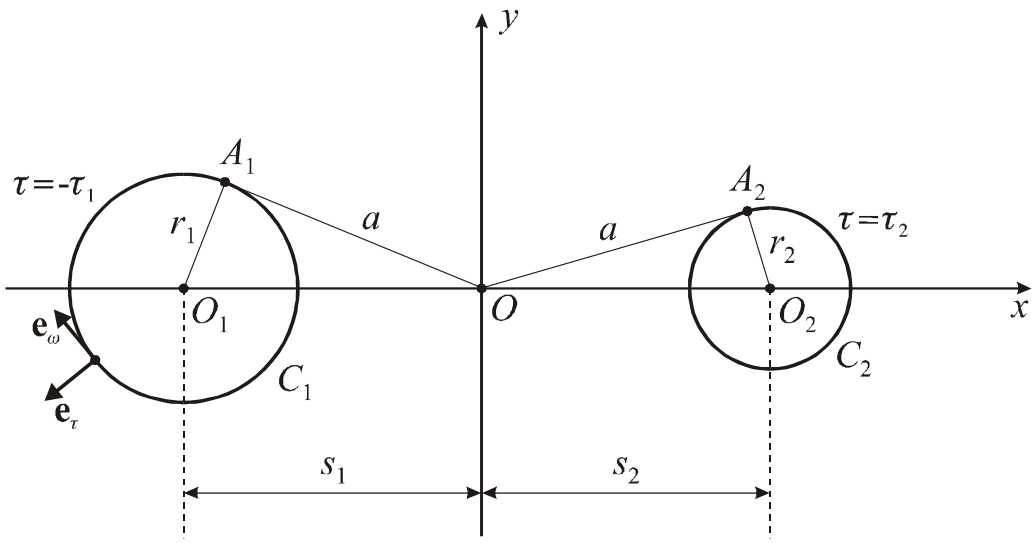

Fig. 7.11. Introduction of bipolar coordinates in the plane *xy*, see Eq. (7.25): the *x*-axis passes through the centers O_1 and O_2 of the contact line projections C_1 and C_2; the coordinate origin O is located in such a way that the two tangents, OA_1 and OA_2, have equal length a.

The two circumferences in Fig. 7.11 correspond to fixed values of the parameter τ, $\tau = -\tau_1$ and $\tau = \tau_2$, where τ_1 and τ_2 are related to the geometrical parameters as follows:

$$\cosh\tau_k = s_k/r_k\,, \qquad \sinh\tau_k = a/r_k \qquad (k = 1,2). \tag{7.29}$$

A substitution of Eqs. (7.29) into Eq. (7.28) yields the known identity $\cosh^2\tau_k - \sinh^2\tau_k = 1$. The τ-lines are a family of circumferences in the plane *xy* determined by the equation [63]:

$$x^2 + (y - a\coth\tau)^2 = a^2/\sinh^2\tau \tag{7.30}$$

Since $\sinh\tau_k \equiv a/r_k$ one realizes that the two circumferences $\tau = -\tau_1$ and $\tau = \tau_2$ have really radii r_1 and r_2, see Fig. 7.11. The parameter a is related to the distance $L = s_1 + s_2$ by means of the expression [19]:

$$a^2 = [L^2 - (r_1 + r_2)^2]\,[L^2 - (r_1 - r_2)^2]/(2L)^2 \tag{7.31}$$

One sees that $a \approx L$ for $L\to\infty$, and $a\to 0$ at close contact, $L\to(r_1 + r_2)$. In bipolar coordinates Eq. (7.6) takes the form [63,14,19]:

$$(\cosh\tau - \cos\omega)^2\left(\frac{\partial^2\zeta}{\partial\tau^2} + \frac{\partial^2\zeta}{\partial\omega^2}\right) = (qa)^2\,\zeta(\tau,\omega) \tag{7.32}$$

For small particles and not too large interparticle separations one has $(qa)^2 << 1$, and then Eq. (7.32) contains a small parameter. In such a case, following the method of the matched asymptotic expansions [73] one can consider an inner and an outer region:

inner region (close to the particles): $(\cosh\tau - \cos\omega)^2 >> (qa)^2$ (7.33)

outer region (far from the particles): $(\cosh\tau - \cos\omega)^2 << (qa)^2$ (7.34)

We seek the solution of Eq. (7.32) for two vertical cylinders, like those depicted in Fig. 7.12. (In Section 7.3 it will be demonstrated that the results for vertical cylinders can be extended to describe the case of spherical particles.) The meniscus slope at the cylinders is determined by the slope angles

$$\psi_k = \pi/2 - \alpha_k, \qquad k = 1,2, \tag{7.35}$$

where α_1 and α_2 are the contact angles. Consequently, the following boundary conditions must be satisfied at the two contact lines [19]:

$$\frac{\partial\zeta}{\partial\tau} = (-1)^k \sqrt{g_{\tau\tau}}\sin\psi_k \qquad \text{for} \quad \tau = (-1)^k\tau_k \qquad (k = 1,2) \tag{7.36}$$

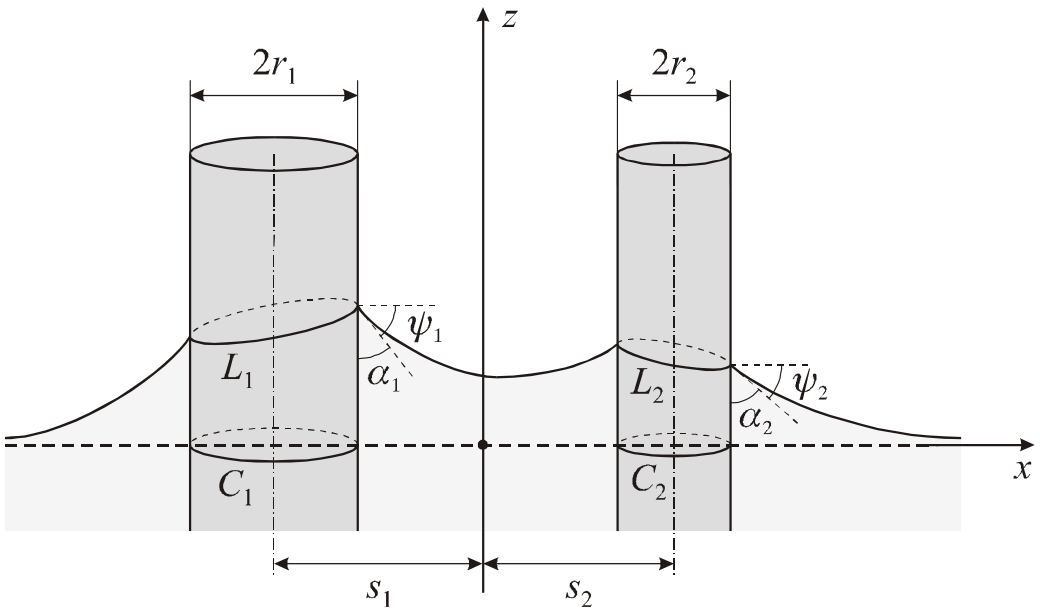

Fig. 7.12. Schematic view of the capillary meniscus around two partially immersed vertical cylinders of radii r_1 and r_2; α_1 and α_2 are contact angles, ψ_1 and ψ_2 are meniscus slope angles at the respective contact lines L_1 and L_2, whose horizontal projections are denoted by C_1 and C_2.

Other boundary condition is the meniscus to level off far from the cylinders:

$$\lim_{r\to\infty}\zeta = 0, \qquad r \equiv \sqrt{x^2 + y^2} \tag{7.37}$$

In Refs. [14] and [19] the method of the matched asymptotic expansions [73] was applied and the solution was found in the form of a compound expansion:

$$\zeta = \zeta^{\text{in}} + \zeta^{\text{out}} - (\zeta^{\text{out}})^{\text{in}} \tag{7.38}$$

where

$$\zeta^{\text{out}} = (Q_1 + Q_2)\mathrm{K}_0(qr) \qquad (Q_k \equiv r_k \sin\psi_k,\ k = 1,2) \tag{7.39}$$

$$(\zeta^{\text{out}})^{\text{in}} = -(Q_1 + Q_2)\ln(\gamma_{\text{e}} qr/2) \qquad \gamma_{\text{e}} = 1.781072418... \tag{7.40}$$

$$\zeta^{\text{in}} = \begin{cases} \zeta_1(\tau,\omega) \text{ for } -\tau_1 \le \tau \le 0 \\ \\ \zeta_2(\tau,\omega) \text{ for } 0 \le \tau \le \tau_2 \end{cases} \tag{7.41}$$

Here γ_{e} is the Euler-Masceroni number, see e.g. Ref. [61] and the functions ζ_1 and ζ_2 are defined as follows [19]:

$$\zeta_k(\tau,\omega) = C_0 + Q_k \ln(2\cosh\tau - 2\cos\omega) + \sum_{n=1}^{\infty} C_n^{(k)} \cosh n[\tau - (-1)^k \tau_k] \cos n\omega \tag{7.42}$$

where the coefficients are given by the expressions

$$C_0 = (Q_1 - Q_2)A - (Q_1 + Q_2)\ln(\gamma_{\text{e}} qr), \qquad A \equiv \sum_{n=1}^{\infty} \frac{1}{n} \frac{\sinh n(\tau_1 - \tau_2)}{\sinh n(\tau_1 + \tau_2)} \tag{7.43}$$

$$C_n^{(k)} = \frac{2}{n}(Q_k - Q_j)\frac{\sinh n\tau_j}{\sinh n(\tau_1 + \tau_2)} \qquad j,k = 1,2;\quad j \ne k,\quad n = 1,2,3,... \tag{7.44}$$

Eqs. (7.39)–(7.44) describe the meniscus profile around two cylinders of different radii supposedly the condition $(qa)^2 << 1$ is satisfied. Such is the case of colloid-sized particles, which represents a physical and practical interest.

For two *identical* cylinders

$$Q_1 = Q_2 = Q, \qquad s_1 = s_2 = s, \qquad r_1 = r_2 = r_c, \qquad \tau_1 = \tau_2 = \tau_c, \tag{7.45}$$

and in such a case Eqs. (7.41)–(7.42) for ζ^{in} considerably simplifies [14,19]:

$$\zeta^{in}(\tau,\omega) = Q\,[\ln(2\cosh\tau - 2\cos\omega) - 2\ln(\gamma_e qr)] \tag{7.46}$$

The above expressions serve as a basis for the quantitative description of the lateral capillary forces between cylindrical and spherical particles (see below). First we will obtain some useful auxiliary expressions for the mean elevation and the shape of the contact line.

7.2.2. MEAN CAPILLARY ELEVATION OF THE PARTICLE CONTACT LINE

As already mentioned, the two contact lines, $\tau = -\tau_1$ and $\tau = \tau_2$, are not perfectly horizontal, that is ζ^{in} depends on ω along the contact line. The deviation from horizontality is small for small particles (thin cylinders) [14]. The mean elevation of the contact lines above the horizontal interface far from the cylinders is [14,19]:

$$h_k = \frac{1}{2\pi r_k}\oint_{C_k} dl\,\zeta^{in}((-1)^k\tau_k,\omega) \qquad k = 1,2. \tag{7.47}$$

Using Eqs. (7.27) and (7.41)–(7.44) one can solve the integral in Eq. (7.47) to obtain [19]:

$$\begin{aligned} h_k &= Q_k\{\tau_k + 2\ln[1-\exp(-2\tau_k)]\} - (Q_1+Q_2)\ln(\gamma_e qa) \\ &+ (Q_1-Q_2)\left[A - (-1)^k\sum_{n=1}^{\infty}\frac{2}{n}\frac{\exp(-n\tau_k)\sinh n\tau_j}{\sinh n(\tau_1+\tau_2)}\right] \qquad (j\neq k,\ \ j,k=1,2) \end{aligned} \tag{7.48}$$

In accordance with Eq. (7.29) τ_k can be expressed in the form:

$$\tau_k = \ln\left(\frac{a}{r_k} + \sqrt{\frac{a^2}{r_k^2}+1}\right), \qquad k = 1,2; \tag{7.49}$$

a and A are given by Eqs. (7.31) and (7.43), respectively. The value of h_k can be both positive and negative.

For two identical cylinders Eq. (7.45) holds and $h_1 = h_2 = h_c$; in this special case Eq. (7.48) considerably simplifies [14]:

$$h_c = Q\left\{\tau_c + 2\ln\left[\frac{1-\exp(-2\tau_c)}{\gamma_e qa}\right]\right\} \qquad \text{(identical cylinders)} \tag{7.50}$$

Note that both Eqs. (7.48) and (7.50) are derived under the assumption, that $(qa)^2 << 1$, which means that both the cylinder radii, r_1 and r_2, and the distance between the cylinders, L, is small compared to the capillary length, q^{-1}. The restriction $qL << 1$ can be overcome applying again the method of the matched asymptotic expansions, as follows.

First of all, we note that in the limit of infinite separation between the two cylinders, $L \to \infty$, the limiting value $h_{k\infty}$ of h_k can be calculated by using the Derjaguin formula [74] for an isolated cylinder:

$$h_{k\infty} = Q_k \ln \frac{4}{\gamma_e q r_k (1+\cos\psi_k)} \approx Q_k \ln \frac{2}{\gamma_e q r_k}, \qquad k = 1,2; \qquad (qr_k)^2 << 1. \qquad (7.51)$$

At the last step we have used the fact that in the considered case of small meniscus slope we have $\sin^2\psi_k << 1$, which implies $\cos\psi_k \approx 1$. In the case of two identical cylinders using Eqs. (7.29) and (7.45) one can represent Eq. (7.50) in the following form [22]:

$$h_c^{\text{in}} = Q \ln \frac{2}{\gamma_e q r_c} + Q \ln \frac{2}{\gamma_e q (s+a)}, \qquad (qa)^2 << 1, \qquad (7.52)$$

without using any approximations. The subscript "in" means that we consider Eq. (7.52) as a limiting expression for h_c in the "inner region" of relatively short interparticle distances, for which $(qa)^2 << 1$. In the complementary "outer region" one can use the superposition approximation of Nicolson (3), see Section 7.1.3, to derive

$$h_c^{\text{out}} = h_{c\infty} + Q\mathrm{K}_0(2qs), \qquad (qa)^2 \geq 1. \qquad (7.53)$$

where $h_{c\infty}$ can be calculated from Eq. (7.51) with $r_k = r_c$. For small values of the argument the K_0 function can be expressed in the form [61,65]:

$$\mathrm{K}_0(x) = \ln \frac{2}{\gamma_e x} + O(x \ln x) \qquad x << 1. \qquad (7.54)$$

Taking into account Eqs. (7.51)–(7.54) one can obtain the leading term in the *compound expansion* for h_c [22]:

$$h_c = h_{c\infty} + Q\mathrm{K}_0(q(s+a)), \qquad (qr_c)^2 << 1. \tag{7.55}$$

One can check that for short distances, $q(s + a) << 1$, Eq. (7.55) reduces to the "inner expansion", Eq. (7.52), whereas for long distances one has $a \approx s$ and Eq. (7.55) reduces to Eq. (7.53). It turns out that Eq. (7.55) predicts the capillary elevation h_c with a good accuracy for the whole range of distances between the two cylinders, from close contact up to infinite separations.

In the case of two dissimilar cylinders, like those depicted in Fig. 7.12, one can obtain a generalization of Eq. (7.55) by using Eq. (7.48) and asymptotic expansions proposed in Ref. [19]:

$$h_k = h_{k\infty} + Q_j\,\mathrm{K}_0(q(s_k + a)), \qquad j \neq k,\ \ j,k = 1,2; \qquad (qr_k)^2 << 1. \tag{7.56}$$

Equation (7.56) is subject to the additional condition $(r_k/s_k)^4 << 1$, which is violated for close distances between the two cylinders. That is the reason why the usage of Eq. (7.48) is recommended for close distances between the two cylinders and Eq. (7.56) can be applied for all other distances. In Section 7.3 we make use of Eqs. (7.55) and (7.56) to quantify the capillary interaction by means of the *energy* approach.

7.2.3. EXPRESSIONS FOR THE SHAPE OF THE CONTACT LINE

Let us begin with the case of two *identical* vertical cylinders. (As already mentioned, in Section 7.3 it will be demonstrated that the results for vertical cylinders can be extended to describe the case of spherical particles.) In view of Eqs. (7.29) and (7.45) one can write

$$\tau_c = \ln(a/r_c + \sqrt{a^2/r_c^2 + 1}) = \ln(s/r_c + \sqrt{s^2/r_c^2 - 1}) = \ln[(a+s)/r_c] \tag{7.57}$$

By means of the last equation one can bring Eq. (7.46) for $\tau = \tau_c$ into the form [22]:

$$\zeta_c^{\mathrm{in}} \equiv \left(\zeta^{\mathrm{in}}\right)_{\tau=\tau_c} = Q\ln\frac{2}{\gamma_{\mathrm{e}} qr_c} + Q\ln\frac{2}{\gamma_{\mathrm{e}} 2qa^2/(s - r_c\cos\omega)} \qquad (qa)^2 << 1. \tag{7.58}$$

$\zeta_c^{\mathrm{in}}(\omega)$ describes the shape of the three-phase contact line at the surface of each cylinder in the "inner region" corresponding to relatively shorter distance between the cylinders, for which $(qa)^2 << 1$. In the complementary case of large separations, $(qa)^2 \geq 1$, one can use the

superposition approximation representing the meniscus shape around a couple of particles as a sum of the deformations, created by two isolated particles. The meniscus around a single axisymmetric particle is described by the Derjaguin equation, $z(r) = Q\mathrm{K}_0(qr)$, see Section 2.2.2. Thus one obtains [22]:

$$\zeta_c^{\mathrm{out}}(\omega) = Q\mathrm{K}_0(qr_r) + Q\mathrm{K}_0(qr_l), \qquad (qa)^2 \geq 1 \tag{7.59}$$

where the superscript "out" means that Eq. (7.59) is valid in the outer asymptotic region of not-too-small interparticle separations, $(qa)^2 \geq 1$, in which the superposition approximation can be applied. The indices *"l"* and *"r"* denote the left- and right-hand side particles, in particular

$$r_l^2 = (x+s)^2 + y^2, \qquad r_r^2 = (x-s)^2 + y^2. \tag{7.60}$$

In the outer region, for relatively long distances, $(r_c/s)^2 << 1$, one can write $a \equiv \sqrt{s^2 - r_c^2} \approx s$ and to rewrite Eq. (7.60) in the form

$$r_l^2 \approx (x+a)^2 + y^2, \qquad r_r^2 \approx (x-a)^2 + y^2. \tag{7.61}$$

Next, for the particle contact line, $(x,y) \in C$, we substitute x and y from Eq. (7.25) into Eq. (7.61) and rearrange the result using Eqs. (7.29) and (7.45); thus we obtain [22]:

$$r_l^2 = \frac{2a^2(s+a)}{s - r_c\cos\omega}, \qquad r_r^2 = \frac{2a^2(s-a)}{s - r_c\cos\omega} \tag{7.62}$$

To find the inner asymptotics of the "outer expansion" in Eq. (7.59) we carry out a transition $a \to 0$ (qr_l, $qr_r \to 0$); then from Eqs. (7.54) and (7.59) we obtain [22]

$$\left(\zeta_c^{\mathrm{out}}\right)^{\mathrm{in}} \approx Q\left(\ln\frac{2}{\gamma_{\mathrm{e}} qr_r} + \ln\frac{2}{\gamma_{\mathrm{e}} qr_l}\right) \tag{7.63}$$

The substitution of Eq. (7.62) into Eq. (7.63) after some algebra gives exactly Eq. (7.58), without any approximations, i.e. $\left(\zeta_c^{\mathrm{out}}\right)^{\mathrm{in}} \equiv \zeta_c^{\mathrm{in}}$. Finally, in keeping with Eq. (7.54) we return back to K_0 function in Eq. (7.58) to obtain a "compound" expression for $\zeta_c(\omega)$, which for small separations reduces to ζ_c^{in}, Eq. (7.58), and for large separations yields ζ_c^{out}, Eq. (7.59) [22]:

$$\zeta_c(\omega) = h_{c\infty} + QK_0\left(\frac{2qa^2}{s - r_c\cos\omega}\right), \qquad (qr_c)^2 << 1, \quad |\nabla_{\mathrm{II}}\zeta|^2 << 1, \tag{7.64}$$

where $h_{c\infty}$ is the Derjaguin's [74] expression for the elevation of the contact line for an isolated axisymmetric particle:

$$h_{c\infty} \approx Q \ln \frac{2}{\gamma_e q r_c} \tag{7.65}$$

cf. Eq. (7.51). Equation (7.64) can be applied for any interparticle distances, characterized by the parameter a, see Eq. (7.31). For $a \to 0$ Eq. (7.64) predicts $\zeta_c(\omega) \to \infty$ for $\omega \neq 0$, i.e. the liquid climbs up in the narrow gap between the two infinitely long vertical cylinders; this limiting result could be qualitatively correct for the considered idealized situation, but it could hardly be quantitatively correct insofar as the presumption for small meniscus slope, $|\nabla_{\mathrm{II}}\zeta|^2 << 1$, is violated for such short distances.

Equation (7.64) can be generalized to describe the shape of the contact lines, $\zeta_{c,1}(\omega)$ and $\zeta_{c,2}(\omega)$, on two cylinders of *different* radii, r_1 and r_2. Applying to Eq. (7.41)–(7.44) the asymptotic procedure described in the Appendix of Ref. [19] one can derive

$$\zeta_{c,k}(\omega) = h_{k\infty} + Q_j K_0\left(\frac{2qa^2}{s_k - r_k \cos\omega}\right), \qquad (qr_k)^2 << 1, \qquad |\nabla_{\mathrm{II}}\zeta|^2 << 1, \qquad (r_k/s_k)^4 << 1 \tag{7.66}$$

($j \neq k$, $j,k = 1,2$), where $h_{k\infty}$ is given by Eq. (7.51). The validity of Eq. (7.66) is limited by one additional condition, $(r_k/s_k)^4 << 1$, as compared with Eq. (7.64); if the latter condition is violated at short interparticle distances, the usage of the more rigorous expressions, Eq. (7.41)–(7.44), is recommended. In Section 7.4 below we make use of Eqs. (7.64) and (7.66) to quantify the capillary interaction by means of the *force* approach.

7.3. ENERGY APPROACH TO THE LATERAL CAPILLARY INTERACTIONS

7.3.1. CAPILLARY IMMERSION FORCE BETWEEN TWO VERTICAL CYLINDERS

We begin with the case of two partially immersed vertical cylinders, Fig. 7.12. According to Eq. (7.16) the free energy (the grand thermodynamic potential) of the system can be expressed as a sum of three terms, W_g, W_w and W_m, which are the contributions of the gravitational energy, the wetting of the cylinder surfaces and the meniscus surface energy, respectively. Below we will separately consider these three contributions.

The meniscus surface energy can be expressed as $W_{\mathrm{m}} = \sigma \Delta A$, see Eq. (7.18). Its contribution to the capillary interaction energy between two cylinders can be written in the form

$$\Delta W_{\mathrm{m}} = \sigma (\Delta A - \Delta A_{\infty}) \tag{7.67a}$$

where ΔA_{∞} is the value of ΔA at infinite distance between the two cylinders. The difference ΔA between the area of the meniscus and the area of its projection on the plane xy can be expressed in the form [14]

$$\Delta A = \int\limits_{S_{\mathrm{m}}} \left[\left(1 + \left| \nabla_{\mathrm{II}} \zeta \right|^2 \right)^{1/2} - 1 \right] ds \tag{7.67b}$$

where ∇_{II} is the gradient operator in the plane xy defined by Eq. (7.2), $ds = dxdy$ is the surface element and the integration is carried out over the projection, S_{m}, of the meniscus on the plane xy. If the meniscus slope is small, the square root in Eq. (7.67b) can be expanded in series

$$\Delta A \approx \tfrac{1}{2} \int\limits_{S_{\mathrm{m}}} (\nabla_{\mathrm{II}} \zeta) \cdot (\nabla_{\mathrm{II}} \zeta) ds \qquad (|\nabla_{\mathrm{II}} \zeta|^2 << 1) \tag{7.68}$$

With the help of the linearized Laplace equation, $\nabla_{\mathrm{II}}^2 \zeta = q^2 \zeta$, one derives [14]:

$$(\nabla_{\mathrm{II}} \zeta) \cdot (\nabla_{\mathrm{II}} \zeta) = \nabla_{\mathrm{II}} \cdot (\zeta \nabla_{\mathrm{II}} \zeta) - \zeta \nabla_{\mathrm{II}}^2 \zeta = \nabla_{\mathrm{II}} \cdot (\zeta \nabla_{\mathrm{II}} \zeta) - q^2 \zeta^2 \tag{7.69}$$

Further, we substitute Eq. (7.69) into Eq. (7.68), and in view of Eq. (7.67a) and the definition $q^2 = \Delta \rho g / \sigma$ we obtain [14]

$$\Delta W_{\mathrm{m}} = \sigma (I_c - I_{c\infty}) - \Delta \rho \, g (I_{\mathrm{v}} - I_{\mathrm{v}\infty}) \tag{7.70}$$

where we have introduced the notation

$$I_c \equiv \tfrac{1}{2} \int\limits_{S_{\mathrm{m}}} ds \nabla_{\mathrm{II}} \cdot (\zeta \nabla_{\mathrm{II}} \zeta) \tag{7.71}$$

$$I_{\mathrm{v}} \equiv \int\limits_{V_{\mathrm{m}}} z dV = \int\limits_{S_{\mathrm{m}}} ds \int\limits_{0}^{\zeta} z dz = \tfrac{1}{2} \int\limits_{S_{\mathrm{m}}} ds \zeta^2 \tag{7.72}$$

V_{m} is the volume comprised between the meniscus surface $z = \zeta(x,y)$ and its projection S_{m} on the plane xy; $I_{c\infty}$ and $I_{\mathrm{v}\infty}$ are the limiting values of I_c and I_{v} for infinite distance ($L \to \infty$) between

the axes of the two vertical cylinders. Equation (7.71) can be rearranged using the Green theorem [14,75]:

$$I_c = \tfrac{1}{2} \sum_{k=1,2} \oint_{C_k} dl\, \tilde{\mathbf{n}} \cdot (\zeta \nabla_{\mathrm{II}} \zeta) \tag{7.73}$$

Here, as usual, the contours C_k (k = 1,2) are the projections of the contact lines L_k on the plane xy; the contour C_k is oriented clock-wise and $\tilde{\mathbf{n}}$ is its running unit normal directed inward; to obtain Eq. (7.73) it has been also used that the integrand $\zeta \nabla_{\mathrm{II}} \zeta$ vanishes at infinity. For two *identical* cylinders one can write $\psi_1 = \psi_2 = \psi_c$, and then from the boundary condition for constant contact angle, Eq. (7.36), it follows

$$\tilde{\mathbf{n}} \cdot \nabla_{\mathrm{II}} \zeta = (-1)^k \frac{1}{\sqrt{g_{\tau\tau}}} \frac{\partial \zeta}{\partial \tau} = \sin \psi_c = \text{const.} \qquad \text{for } \tau = (-1)^k \tau_c \tag{7.74}$$

In such a case Eq. (7.73) reduces to

$$I_c = \sin \psi_c \oint_{C_1} dl \zeta = 2\pi r_c h_c \sin \psi_c = 2\pi Q h_c; \qquad h_c \equiv \frac{1}{2\pi r_c} \oint_{C_1} dl \zeta \tag{7.75}$$

cf. Eqs. (7.9), (7.45) and (7.47). In this way the mean elevation of the contact line h_c enters the expression for the energy of capillary interaction. Using Eq. (7.75) one can represent the meniscus surface energy, Eq. (7.70), in the form

$$\Delta W_{\mathrm{m}} = 2\pi\sigma Q(h_c - h_{c\infty}) - \Delta\rho\, g(I_{\mathrm{v}} - I_{\mathrm{v}\infty}) \tag{7.76}$$

The gravitational potential energy, W_{g}, given by Eq. (7.17) varies only because the shape of the interface between phases I and II changes when the distance between the two cylinders is altered; the mass centers of the cylinders are not supposed to change their positions, $Z_k^{(c)}$. Since the interface is flat far from the cylinders, the hydrostatic pressures in the two neighboring phases can be expressed in the form $P_Y = P_0 - \rho_Y g z$, where P_0 is the pressure at the level z = 0, see Fig. 7.12. Then Eq. (7.17) reduces to

$$W_{\mathrm{g}} = \text{const.} - \sum_{Y=\mathrm{I,II}} \int_{V_Y} P_Y dV = \text{const.} + \Delta\rho g \int_{V_{\mathrm{m}}} z dV = \text{const.} + \Delta\rho g I_{\mathrm{v}}\ ; \tag{7.77}$$

here, as usual, $\Delta\rho \equiv \rho_{\rm I} - \rho_{\rm II}$; we have used Eq. (7.72) and the fact that the total volume of the system, $V_{\rm I} + V_{\rm II}$, is constant. Then the contribution of the gravitational potential energy to the capillary interaction energy becomes [14]

$$\Delta W_{\rm g} = \Delta\rho\, g(I_{\rm v} - I_{\rm v\infty}) \tag{7.78}$$

Summing up Eqs. (7.76) and (7.78) one obtains

$$\Delta W_{\rm m} + \Delta W_{\rm g} = 2\pi\sigma Q(h_c - h_{c\infty}) \tag{7.79}$$

Since Q and $(h_c - h_{c\infty})$ have the same sign, then the combined contribution of the meniscus surface energy and the gravitational potential energy, $\Delta W_{\rm w} + \Delta W_{\rm g}$, is always positive, i.e. it corresponds to repulsion. This is related to the fact that the capillary rise h_c increases when the cylinders come closer; simultaneously the deviation of the meniscus from planarity increases, which is energetically unfavorable.

The energy of wetting, given by Eq. (7.18), can be expressed as follows

$$W_{\rm w} = \sum_{k=1}^{N} \sum_{Y={\rm I,II}} \sigma_{kY} A_{kY} = 2(\sigma_{\rm I} - \sigma_{\rm II}) \oint_{C_1} dl\zeta + \text{const.} = 4\pi r_c(\sigma_{\rm I} - \sigma_{\rm II})h_c + \text{const.} \tag{7.80}$$

cf. Eq. (7.75); here we have used the fact that for identical cylinders $\sigma_{kY} = \sigma_Y$ ($k = 1,2$; $Y = {\rm I,II}$). The contribution of the energy of wetting to the capillary interaction energy is

$$\Delta W_{\rm w} \equiv W_{\rm w} - W_{\rm w\infty} = 4\pi r_c(\sigma_{\rm I} - \sigma_{\rm II})(h_c - h_{c\infty}) \tag{7.81}$$

$\Delta W_{\rm w}$ is defined in such a way that $\Delta W_{\rm w} \to 0$ for large distances, $L \to \infty$. We assume that the Young equation (see Section 2.3.1) holds,

$$\sigma_{\rm II} - \sigma_{\rm I} = \sigma\cos\alpha = \sigma\sin\psi_c\,, \tag{7.82}$$

and then Eq. (7.81) becomes

$$\Delta W_{\rm w} = -4\pi\sigma r_c\,(h_c - h_{c\infty})\sin\psi_c = -4\pi\sigma Q\,(h_c - h_{c\infty}) \tag{7.83}$$

As mentioned above, Q, and $(h_c - h_{c\infty})$ have the same sign, then the contribution of the wetting energy, $\Delta W_{\rm w}$, is always negative, i.e. it corresponds to attraction. The comparison between Eqs. (7.79) and (7.83) shows that $\Delta W_{\rm w}$ is two times larger by magnitude than $\Delta W_{\rm m} + \Delta W_{\rm g}$;

consequently, the work of wetting $\Delta W_{\rm w}$ determines the sign and the trend of the total capillary interaction energy [14]:

$$\Delta\Omega = \Delta W_{\rm w} + \Delta W_{\rm m} + \Delta W_{\rm g} = -2\pi\sigma Q\,(h_c - h_{c\infty}) \tag{7.84}$$

Thus the intuitive assumption that the interaction energy can be identified with a half of the work of wetting (wetting of one of the two cylinders), which was used in Section 7.1.3 to obtain Eq. (7.11), turns out to be correct. The substitution of Eq. (7.55) into Eq. (7.84) gives the dependence of the interaction energy $\Delta\Omega$ on the distance L between the axes of the two identical vertical cylinders:

$$\Delta\Omega = -2\pi\sigma Q^2 {\rm K}_0(q(s+a)) \qquad\qquad (qr_c)^2 << 1. \tag{7.85}$$

Note that $a = \sqrt{s^2 - r_c^2}$ and $s = L/2 - r_c$. Differentiating Eq. (7.85) one obtains the capillary immersion force:

$$F \equiv -\frac{d\Delta\Omega}{dL} = -2\pi\sigma Q^2 \frac{a+s}{2a} q{\rm K}_1(q(s+a)) \qquad\qquad (qr_c)^2 << 1. \tag{7.86}$$

For $(r_c/s)^2 << 1$ one has $s \approx a \approx L/2$ and then Eqs. (7.85) and (7.86) reduce to their long-distance asymptotic forms, which can be obtained by means of the superposition approximation, see Section 7.1.3 above:

$$\Delta\Omega = -2\pi\sigma Q^2 {\rm K}_0(qL), \qquad F = -2\pi\sigma Q^2 q{\rm K}_1(qL) \qquad [(qr_c)^2 << 1,\ (r_c/s)^2 << 1]. \tag{7.87}$$

If the two cylinders have different radii, r_1 and r_2, see Fig. 7.12, Eq. (7.84) can be generalized following the same scheme of derivation [19]:

$$\Delta\Omega = -\,\pi\sigma \sum_{k=1,2} Q_k\,(h_k - h_{k\infty}), \qquad\qquad (Q_k = r_k \sin\psi_k) \tag{7.88}$$

The dependence of $\Delta\Omega$ vs. distance L can be obtained substituting the respective expression for h_k, Eq. (7.48) or Eq. (7.56), into Eq. (7.88). For example, the combination of Eqs. (7.56) and (7.88) yields

$$\Delta\Omega = -\,\pi\sigma Q_1 Q_2 \sum_{k=1,2} {\rm K}_0\,(q(s_k + a)), \qquad\qquad [(qr_k)^2 << 1,\ (r_k/s)^4 << 1], \tag{7.89}$$

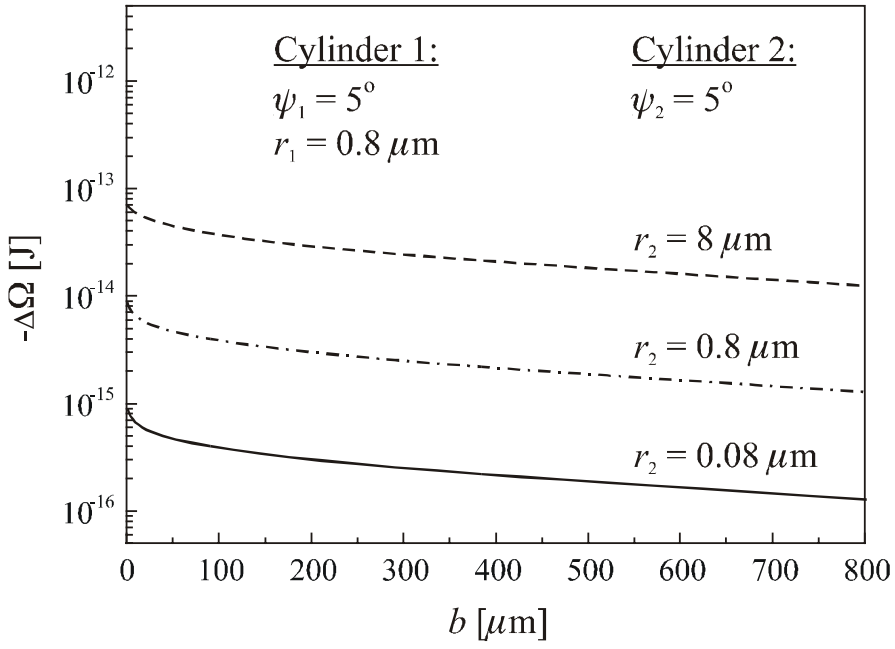

Fig. 7.13. Calculated energy of capillary attraction $\Delta\Omega$ vs. the distance b between the surfaces of two vertical cylinders. The meniscus slope angles are $\psi_1 = \psi_2 = 5°$; the radius of the first cylinder is $r_1 = 0.8$ μm; the curves correspond to three values of the radius r_2 of the second cylinder, which are given in the figure [19].

which reduces to Eq. (7.11) in the limiting case of long distances ($s_k \approx a \approx L/2$). Note that the dependence of a on L is given by Eq. (7.31) and that $s_k = \sqrt{r_k^2 + a^2}$.

As an illustration Fig. 7.13 represents the dependence of $\Delta\Omega$ on the surface-to-surface separation $b \equiv L - r_1 - r_2$ between two vertical cylinders of different radii, r_1 and r_2, but of equal contact angles. $\Delta\Omega$ is calculated from Eqs. (7.48) and (7.88) [19]. As could be expected $\Delta\Omega$ is negative (corresponds to attraction) and $|\Delta\Omega|$ decreases with the increase of the separation b. As seen in Fig. 7.13, $|\Delta\Omega|$ is much larger than the thermal energy $kT \approx 4 \times 10^{-21}$ J. The same is true for spherical particles (instead of cylinders) – see below.

7.3.2. CAPILLARY IMMERSION FORCE BETWEEN TWO SPHERICAL PARTICLES

Now our system is a flat horizontal solid surface covered with a liquid layer of thickness l_0. Following Ref. [19] we consider two spheres of radii R_1 and R_2 which protrude from the liquid layer (Fig. 7.14), i.e.

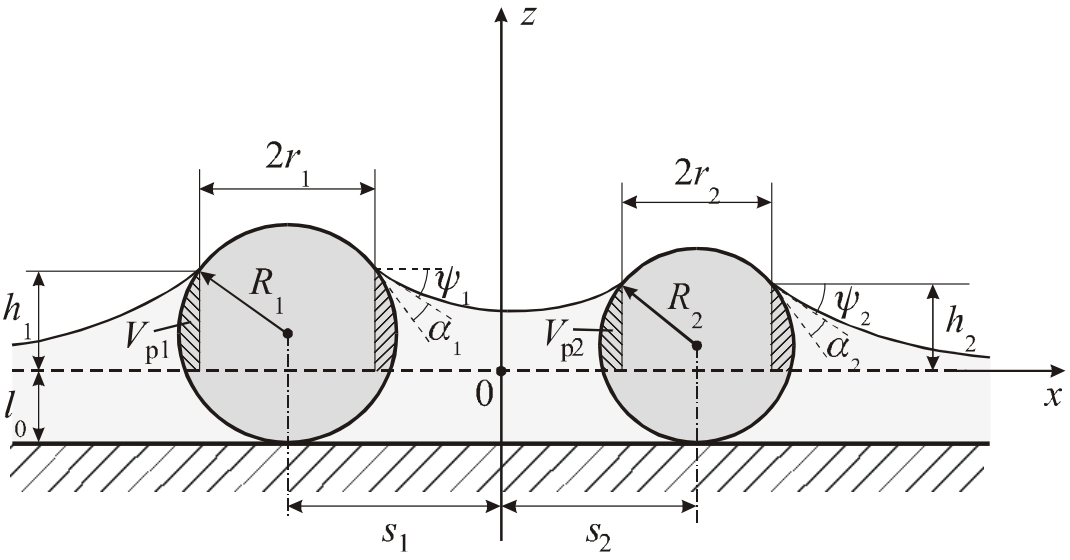

Fig. 7.14. Sketch of the capillary meniscus around two spherical particles of radii R_1 and R_2, which are immersed partially in a wetting liquid film, whose thickness far from the particles is uniform and equal to l_0; h_1 and h_2 denote the capillary elevation of the meniscus at the respective particle contact line; α_k and ψ_k is contact angle and meniscus slope angle, respectively (k = 1,2).

$$l_0 < \min(2R_1,2R_2); \tag{7.90}$$

Our considerations are restricted to small particles and small meniscus slopes at the contact lines:

$$(qR_k) << 1, \qquad \sin^2\psi_k << 1, \qquad k = 1,2. \tag{7.91}$$

In this case the projections of the contact lines in the plane xy can be treated approximately as circumferences of radii r_1 and r_2, see Ref. [14] for details. Instead of Eq. (7.35) now we have

$$\psi_k = \arcsin(r_k/R_k) - \alpha_k, \qquad k = 1,2; \tag{7.92}$$

see Fig. 7.14. Let us mention in advance that when the two particles are small, i.e. $(qR_k) << 1$, they create small meniscus slope, that is the second condition in Eq. (7.91), $\sin^2\psi_k << 1$, is automatically satisfied, irrespective of the values of the contact angles α_1 and α_2.

In the cases of two spheres (Fig. 7.14), unlike the case of two vertical cylinders, the radius of the contact line r_k and the slope angle ψ_k (k = 1,2) vary with the interparticle distance, $L = s_1 + s_2$. This is due to the fact that the increase of the wet area of each particle in Fig. 7.14 is accompanied with a shrinkage of the contact line. The latter fact has to be accounted for in the

expression for the meniscus surface energy, Eq. (7.76), which can be generalized to the case of two different particles as follows [19]:

$$\Delta W_{\mathrm{m}} = \pi\sigma \sum_{k=1,2} \left(Q_k h_k - Q_{k\infty} h_{k\infty} - r_k^2 + r_{k\infty}^2 \right) - \Delta\rho g (I_{\mathrm{v}} - I_{\mathrm{v}\infty}) \tag{7.93}$$

As before, the subscript "∞" denotes the value of the respective quantity at infinite interparticle separation, $L \to \infty$. The term $r_k^2 - r_{k\infty}^2$ accounts for the fact that the meniscus area alters when the radius of the contact line varies; the integral I_{v} is given again by Eq. (7.72).

Since the two particles (Fig. 7.14) move only in horizontal direction, their gravitational potential energy does not change with L. However, the gravitational energy of the two fluid phases varies because of the dependence of the meniscus shape on L. The generalization of Eq. (7.78) to the case of two different spherical particles reads [19]:

$$\Delta W_{\mathrm{g}} = \Delta\rho g (I_{\mathrm{v}} - I_{\mathrm{v}\infty} - \Delta I_p) \tag{7.94}$$

where ΔI_p is a small correction accounting for the gravitational potential energy of the liquid displaced by a portion of the particle volume, denoted by V_{p1} and V_{p2} in Fig. 7.14:

$$\Delta I_p = \sum_{k=1,2} \left(\int_{V_{pk}} |z| \, dV - \int_{V_{pk(\infty)}} |z| \, dV \right) = \Delta I_1 + \Delta I_2 \tag{7.95}$$

Using geometrical considerations one can derive an explicit expression for ΔI_k [19]:

$$\Delta I_k = \tfrac{\pi}{2} \left\{ \tfrac{1}{2} \left(h_k^2 - h_{k\infty}^2 \right) \left(2l_0 (2R_k - l_0) - h_k^2 - h_{k\infty}^2 \right) + \tfrac{4}{3} (R_k - l_0) \left(h_k^3 - h_{k\infty}^3 \right) - r_k^2 h_k^2 + r_{k\infty}^2 h_{k\infty}^2 \right\} \tag{7.95a}$$

It turns out that the contribution of ΔI_p is always negligible for small particles, that is for $(qr_k)^2 << 1$. Again by using geometrical considerations one can derive that the areas of particle 'k' wet by phases I and II are respectively

$$A_{k\mathrm{I}} = 2\pi R_k (h_k + l_0) \quad \text{and} \quad A_{k\mathrm{II}} = 2\pi R_k [2R_k - (h_k + l_0)] \qquad (k = 1,2) \tag{7.96}$$

Then in view of Eq. (7.18) and the Young equation, $\sigma_{k,\mathrm{II}} - \sigma_{k,\mathrm{I}} = \sigma \cos\alpha_k$, one obtains a counterpart of Eq. (7.83) for spherical particles:

$$\Delta W_{\mathrm{w}} = -2\pi\sigma \sum_{k=1,2} R_k \, (h_k - h_{k\infty}) \cos\alpha_k \tag{7.97}$$

A summation of Eqs. (7.93), (7.94) and (7.97) finally yields an expression for the energy of capillary interaction between the two partially immersed spheres [14,19]:

$$\Delta\Omega = -\pi\sigma\sum_{k=1}^{2}\left\{2R_k(h_k - h_{k\infty})\cos\alpha_k - Q_k h_k + Q_{k\infty}h_{k\infty} + r_k^2 - r_{k\infty}^2\right\} - \Delta\rho g\Delta I_p \tag{7.98}$$

Further, the capillary immersion force between the two particles can be calculated by differentiation of Eq. (7.98): $F = -d\Delta\Omega/dL$. The numerical calculations show that the wetting term, $R_k(h_k - h_{k\infty})\cos\alpha_k$, in Eq. (7.98) is predominant and determines the sign and the magnitude of the attractive capillary immersion force. Since $\cos\alpha_k$ is the largest for contact angle $\alpha_k = 0°$, completely "hydrophilic" particles experience a relatively strong capillary *immersion* force when captured in a liquid film. This is understandable, because hydrophilic particles also deform the film surface(s) when the film thickness l_0 is smaller than the particle diameter $2R_k$, as it is in Fig. 7.14. Note however, that hydrophilic particles (of density higher than that of water) cannot experience capillary *flotation* force, see Fig. 7.1a, because they cannot float on the aqueous surface, but instead they sink into the water phase.

To compute the dependence of $\Delta\Omega$ vs. L one has to first calculate the values of some geometric parameters. The following *procedure of calculations* has been proposed in Refs. [14,19]:

The input geometrical parameters are the distance between the centers of the two spheres, L, the thickness of the layer far from the particles, l_0, the particle radii R_k and contact angles α_k, ($k = 1,2$).

From the equation of the particle spherical surface one calculates the contact radius $r_{k\infty}$ of an isolated particle for a given value of the mean elevation $h_{k\infty}$:

$$r_{k\infty}(h_{k\infty}) = [(l_0 + h_{k\infty})(2R_k - l_0 - h_{k\infty})]^{1/2} \tag{7.99}$$

Next from Eq. (7.92) one determines $\psi_{k\infty}(h_{k\infty}) = \arcsin(r_{k\infty}(h_{k\infty})/R_k) - \alpha_k$. The calculated values of $r_{k\infty}$ and $\psi_{k\infty}$ are finally substituted into the Derjaguin equation (7.51)

$$h_{k\infty} = -r_{k\infty}(h_{k\infty})\sin\psi_{k\infty}(h_{k\infty})\ln[\gamma_e q r_{k\infty}(h_{k\infty})/2], \tag{7.100}$$

which is solved numerically to determine $h_{k\infty}$ (as well as $r_{k\infty}$, $\psi_{k\infty}$ and $Q_{k\infty} = r_{k\infty}\sin\psi_{k\infty}$).

Further, h_k, r_k and ψ_k are determined in the following way. From Eq. (7.99) (with r_k, h_k instead of $r_{k\infty}$, $h_{k\infty}$) one calculates $r_k(h_k)$ for each given h_k. Then in view of Eq. (7.92) one calculates $\psi_k(h_k) = \arcsin(r_k(h_k)/R_k) - \alpha_k$. The obtained values of r_k and ψ_k are finally substituted into Eq. (7.48) or Eq. (7.56), which along with Eqs.(7.9), (7.31) and (7.49) determines h_k as a function of L, r_k, and ψ_k:

$$h_k = \Phi_k(L; r_1(h_1), r_2(h_2), \psi_1(h_1), \psi_2(h_2)), \qquad k = 1,2. \tag{7.101}$$

Equation (7.101) for k = 1,2 represents a set of two equations for determining h_1 and h_2 for each given interparticle distance L. In Ref. [19] h_1 and h_2 have been determined by numerical minimization of the function

$$G(h_1, h_2) \equiv \sum_{k=1,2} [h_k - \Phi_k(L; r_1(h_1), r_2(h_2), \psi_1(h_1), \psi_2(h_2))]^2 \tag{7.102}$$

In view of Eq. (7.101) the minimum value of $G(h_1, h_2)$ is zero. The couple (h_1*, h_2*) satisfying the equation $G(h_1, h_2) = 0$ is the sought for solution for $h_1(L)$ and $h_2(L)$, which is to be further substituted in Eq. (7.98) to calculate the interaction energy $\Delta\Omega(L)$. To find (h_1*, h_2*) in Ref. [19] h_1 and h_2 have been varied within the limits $-l_0 < h_k < 2R_k - l_0$, k = 1,2, using the method of Hooke and Jeeves [76].

In the case of two *identical* spherical particles the calculation procedure is similar but simpler: having in mind that $a = (s^2 - r_c^2)^{1/2}$ and $s = L/2$, Eq. (7.55) [or Eq. (7.50) along with Eq. (7.57)] provide an equation for determining h_c:

$$h_c = \Phi(L; r_c(h_c), \psi_c(h_c)), \tag{7.103}$$

where the functions $r_c(h_c)$ and $\psi_c(h_c)$ are determined in the same way as for the case of two different particles, viz. from Eq. (7.99) with r_c, h_c, and R instead of $r_{k\infty}$, $h_{k\infty}$ and R_k, and from the relationship $\psi_c(h_c) = \arcsin(r_c(h_c)/R) - \alpha$. Further, $\Delta\Omega$ can be calculated either from Eq. (7.84), or from Eq. (7.85) with $Q = r_c \sin\psi_c$ is to be computed with the values of r_c and ψ_c obtained for each L by solving Eq. (7.103).

As an illustration in Fig. 7.15 we present the calculated capillary interaction energy $\Delta\Omega$ as a function of the distance L between the centers of two identical hydrophilic spherical particles of radius R = 0.8 μm and contact angle α = 0, which are confined in a wetting film (see Fig. 7.1b).

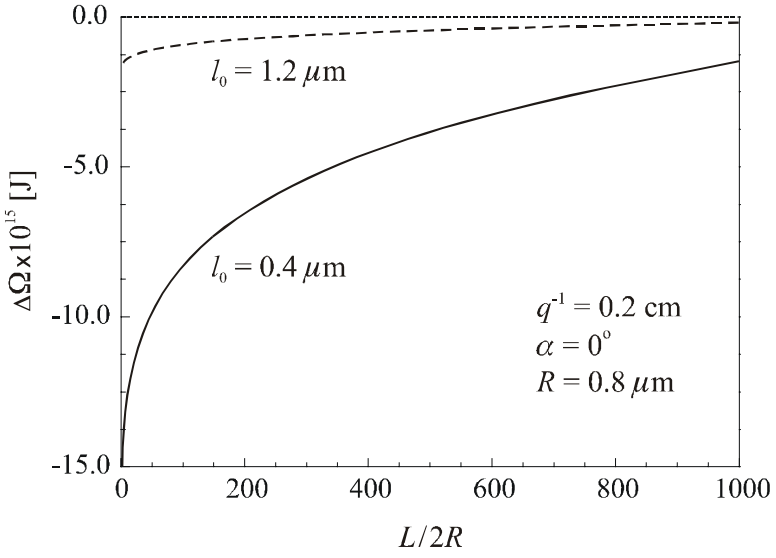

Fig. 7.15. Theoretical dependence of the capillary interaction energy $\Delta\Omega$ vs. $L/2R$, calculated in Ref. [14] for two identical spheres of radius R = 0.8 μm separated at a center-to-center distance L. The spheres are hydrophilic (α = 0°) and are partially immersed in a liquid layer, whose thickness far from the particles is uniform and equal to l_0; the two curves correspond to l_0 = 0.4 and 1.2 μm; the capillary length is q^{-1} = 0.2 cm.

The thickness of the liquid layer far from the particles is taken to be l_0 = 1.2 and 0.4 μm; the capillary length is q^{-1} = 0.2 cm. For l_0 = 1.2 μm the particles create a relatively small deformation of the upper surface of the wetting film, whereas for l_0 = 0.4 μm the deformation is greater. Correspondingly, the magnitude of $\Delta\Omega$ is greater for l_0 = 0.4 μm, see Fig. 7.15.

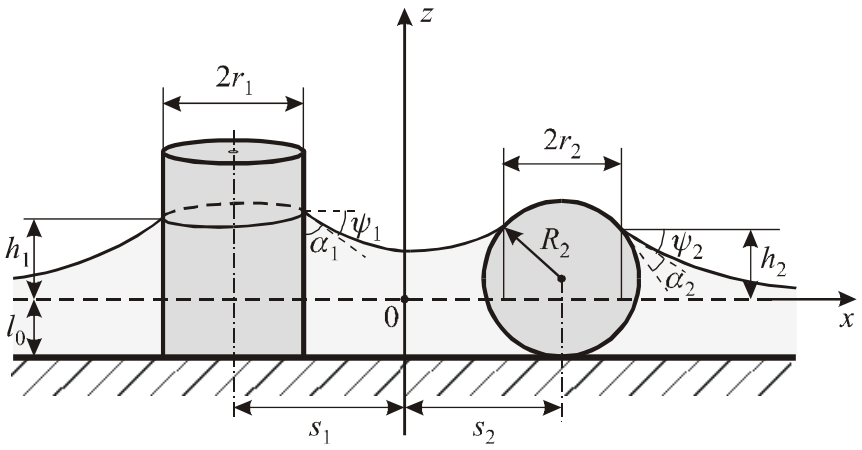

Fig. 7.16. Sketch of a vertical cylinder of radius r_1 and sphere of radius R_2, which are partially immersed in a liquid layer, whose thickness far from the particles is uniform and equal to l_0; r_2 and h_2 are the radius of the particle contact line and its capillary elevation; α_k and ψ_k are contact angle and meniscus slope angle, respectively (k = 1,2).

For both values of l_0 in Fig. 7.15 the interaction energy $\Delta\Omega$ is much greater than the thermal energy $kT \approx 4 \times 10^{-21}$ J. As expected, $\Delta\Omega$ is negative and corresponds to attraction, which turns out to be rather long-ranged: even at distance $L/2R = 1000$, $\Delta\Omega$ is considerably larger than kT [14]. Such a long-range attraction would lead to two-dimensional disorder-order phase transition and formation of ordered clusters or larger domains of particles depending on the experimental conditions; in fact, this has been observed experimentally [11,12,27-29]; see Chapter 13.

7.3.3. CAPILLARY IMMERSION FORCE BETWEEN SPHERICAL PARTICLE AND VERTICAL CYLINDER

The method described above can be directly applied to calculate the capillary interaction between a vertical cylinder and a partially immersed sphere [19]. The system is depicted in Fig. 7.16. The geometrical parameters belonging to the cylinder and the sphere are denoted by indices 1 and 2, respectively. In particular, r_1 and R_2 denote the radii of the cylinder and the sphere; α_k and ψ_k (k = 1,2) are the respective contact and meniscus slope angles, see Fig. 7.16; r_2 and L have the same meaning as in the previous section; a can be calculated from Eq. (7.31). Again we will make use of the assumptions for small particles, $(qr_k)^2 << 1$, and small meniscus slope, $\sin^2\psi_k << 1$. Then following the procedures of derivation of the interaction energy for two cylinders, Eq. (7.88), and for two spheres, Eq. (7.98), one can obtain the following expression for the energy of capillary interaction between a vertical cylinder and a sphere [19]:

$$\Delta\Omega = -\pi\sigma[(h_1 - h_{1\infty})r_1 \sin\psi_1 - Q_2 h_2 + Q_{2\infty} h_{2\infty} + 2R_2(h_2 - h_{2\infty})\cos\alpha_2 + r_2^2 - r_{2\infty}^2] - \Delta\rho g \Delta I_2 \quad (7.104)$$

where ΔI_2 is defined by Eq. (7.95a) for k = 2. The parameters $r_{2\infty}$, $\psi_{2\infty}$ and $h_{2\infty}$ can be determined from Eqs. (7.99) and (7.100) for k = 2. $h_{1\infty}$ can be calculated directly from Eq. (7.51). h_1 and h_2 can be calculated using Eqs. (7.101) and (7.102); simultaneously r_2 and ψ_2 are determined; the numerical procedure is simpler than that for two spheres because of the constancy of some parameters: for the cylinder r_1 = const and $\psi_1 = \pi/2 - \alpha_1$ = const.

As an illustration Fig. 7.17 presents the calculated dependence of the capillary interaction energy $\Delta\Omega$ on the distance L between a vertical cylinder of radius r_1 = 0.5 μm and a sphere of contact angle $\alpha_2 = 10°$; the values of the other parameters are denoted in the figure. The three

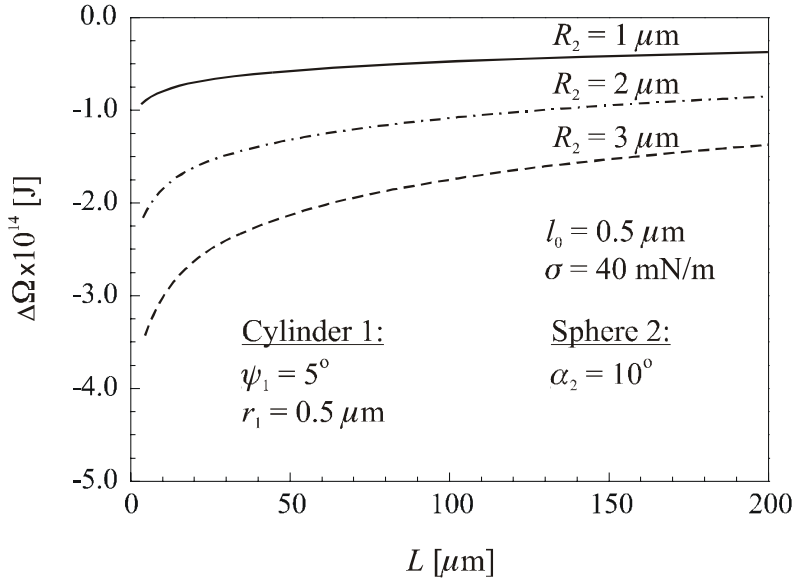

Fig. 7.17. Theoretical dependence of the capillary interaction energy $\Delta\Omega$ vs. the distance $L = s_1 + s_2$, calculated in Ref. [19] for the configuration of cylinder and sphere depicted in Fig. 7.16. The three curves correspond to various values of the particle radius R_2 denoted in the figure; the values of the other parameters are $r_1 = 0.5$ μm, $\psi_1 = 5°$, $\alpha_2 = 10°$, $l_0 = 0.5$ μm, and $\sigma = 40$ mN/m.

curves correspond to three values of the particle radius R_2. One sees that $\Delta\Omega$ is negative (corresponds to attraction) and $|\Delta\Omega|$ increases with the increase of particle radius R_2 at fixed thickness l_0 of the wetting film. Again $|\Delta\Omega|$ is much larger than the thermal energy kT; that is the capillary force prevails over the Brownian force exerted on the particle.

7.3.4. CAPILLARY INTERACTIONS AT FIXED ELEVATION OF THE CONTACT LINE

All cases considered in the previous sections of this chapter correspond to the boundary condition of fixed contact angle at the particle surface. In particular, the obtained solution of the Laplace equation, Eqs. (7.38)–(7.44), satisfies the boundary condition for constant contact angle: Eq. (7.36) along with Eq. (7.35) for cylinders, or with Eq. (7.92) for spheres.

In the present section, following Ref. [21], we consider another physical situation: fixed meniscus *position* (instead of fixed meniscus *slope*) at the contact line. As shown schematically in Fig. 7.18a,b this can happen when the contact line is located at some edge at the particle surface. Other possibility is the contact line to be attached to the boundary between hydrophilic and hydrophobic domains of the surface, as sketched in Fig. 7.18c; similar is the configuration

of two membrane proteins incorporated in a lipid bilayer, which is considered in details in Chapter 10 below. Note that in the case of fixed position of the contact line, the variation in the meniscus shape due to a change in the distance L is accompanied by a *hysteresis* of the contact angle (see Section 2.3.4), i.e. by a variation of the meniscus slope angle (rather than meniscus elevation) at the contact line.

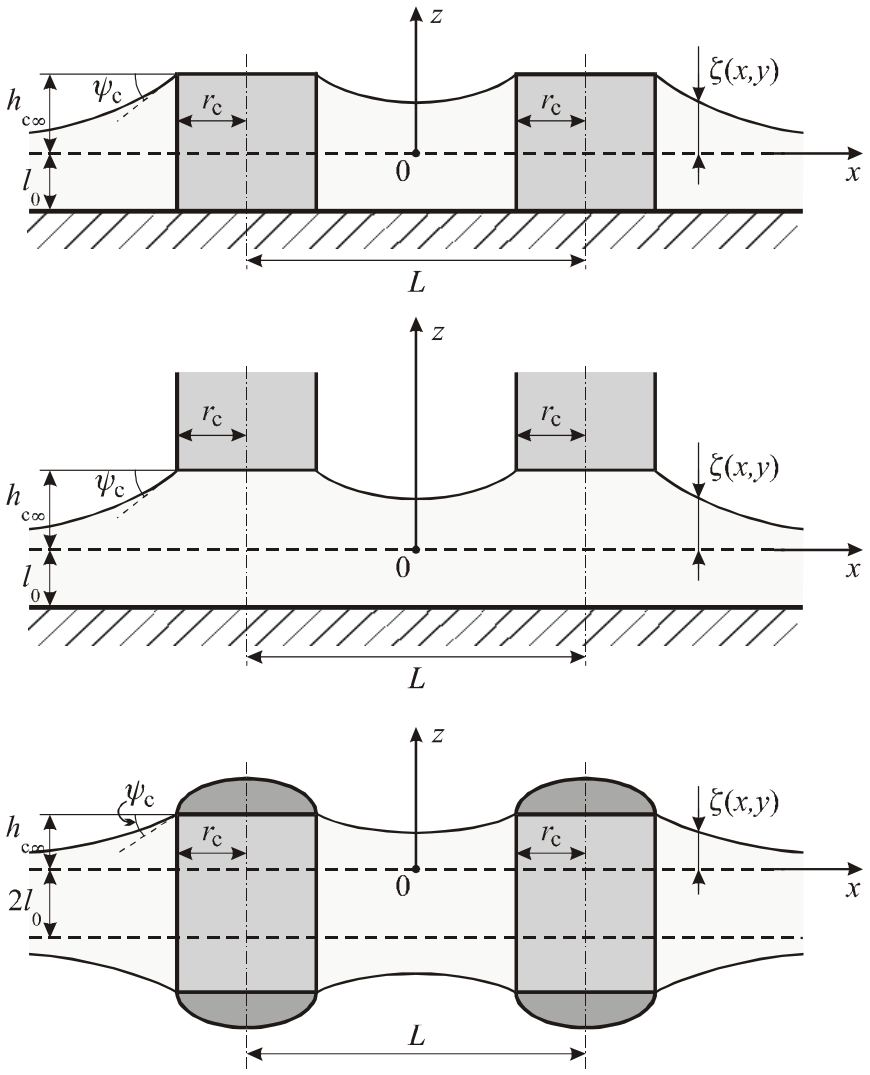

Fig. 7.18. Examples for capillary interaction at fixed elevation $h_{c\infty}$ of the contact line: (a) two cylinders or disks immersed in a liquid layer; (b) two vertical cylinders whose lower bases are attached to a liquid surface; (c) two particles in an emulsion film – the contact lines are attached to the boundaries between the hydrophilic and hydrophobic domains on the particle surface (shown with different shadowing). Since the contact lines are immobilized, the energy of wetting does not contribute to the capillary interaction unlike the case of mobile contact lines shown in Figs. 7.12, 7.14 and 7.16.

Let us consider the meniscus around two *identical* axisymmetric bodies like these depicted in Fig. 7.18. Note that the exact geometry of the bodies (spheres, cylinders, etc.) is not important insofar as the contact line is circular and fixed at the surface of the respective axisymmetric bodies. The derivation of the expression for the capillary interaction energy $\Delta\Omega$ follows exactly Eqs. (7.67)–(7.79) with the only difference that Eq. (7.74) does not hold and Eq. (7.75) takes the alternative form

$$I_c = h_{c\infty} \oint_{C_1} dl(\tilde{\mathbf{n}} \cdot \nabla_{\mathrm{II}} \zeta) = 2\pi r_c h_{c\infty} \sin\Psi_c; \quad \sin\Psi_c \equiv \frac{1}{2\pi r_c} \oint_{C_1} dl(\tilde{\mathbf{n}} \cdot \nabla_{\mathrm{II}} \zeta) \tag{7.105}$$

($\zeta \equiv h_{c\infty}$ at the contact line). For that reason, instead of Eq. (7.79) one obtains [21]

$$\Delta\Omega = \Delta W_{\mathrm{m}} + \Delta W_{\mathrm{g}} = 2\pi\sigma r_c h_{c\infty}[\sin\Psi_c(\mathrm{L}) - \sin\Psi_{c\infty}] \qquad \text{(fixed elevation)} \tag{7.106}$$

We have taken into account the fact that there is no change in the energy of wetting, $\Delta W_{\mathrm{w}} \equiv 0$, when the contact line is fixed, cf. Eq. (7.16). [In the case of symmetric film, Fig. 7.18c, there are two deformed interfaces and consequently the interaction energy is twice $\Delta\Omega$ as given by Eq. (7.106).] In spite of the fact that Eq. (7.106) does not include a direct contribution from the work of wetting, ΔW_{w}, the interaction energy $\Delta\Omega$ is again connected to the special wetting properties of the particle surface due to the fixed position of the contact line, which bring about meniscus deformations and give rise to a non-zero contribution from the meniscus surface energy and the gravitational energy, $\Delta W_{\mathrm{m}} + \Delta W_{\mathrm{g}}$.

To find the profile of the capillary meniscus we will use again bipolar coordinates (τ, ω) in the plane *xy*, see Eq. (7.25). The projections of the two contact lines on the plane *xy* are two circumferences $\tau = \pm\tau_c$ of radius r_c, see Eq. (7.57) where $a = (s^2 - r_c^2)^{1/2}$ and $s = L/2$. The mathematical description of the capillary interaction at fixed position (elevation) of the contact line demands to find a solution of Laplace equation, which satisfies the following (inner) boundary condition

$$\zeta(\tau = \pm\tau_c, \omega) = h_{c\infty} = \text{const} \qquad \text{(fixed elevation of the contact line)} \tag{7.107}$$

The other (the outer) boundary condition is the meniscus to level off at infinity, that is Eq. (7.37) to be satisfied. We seek a solution of Eq. (7.32) satisfying the aforementioned two

boundary conditions. In Ref. [21] inner and outer asymptotic regions are considered, cf. Eqs. (7.33)–(7.34), and a compound solution, $\zeta = \zeta^{\text{in}} + \zeta^{\text{out}} - (\zeta^{\text{out}})^{\text{in}}$, is obtained, in which

$$\zeta^{\text{in}} = h_{c\infty} + A_c \ln(2\cosh\tau - 2\cos\omega) - \tau_c + A_c \sum_{n=1}^{\infty} \frac{2\cosh n\tau}{n\cosh n\tau_c} \exp(-n\tau_c)\cos n\omega \tag{7.108}$$

$$\zeta^{\text{out}} = 2A_c \mathrm{K}_0(qr), \qquad r = (x^2 + y^2)^{1/2} \tag{7.109}$$

$$(\zeta^{\text{out}})^{\text{in}} = -2A_c \ln(\gamma_{\text{e}} qr/2) \tag{7.110}$$

Here, as usual, $\gamma_{\text{e}} = 1.781072418...$ ($\ln\gamma_{\text{e}} = 0.577...$) is the constant of Euler-Masceroni [61] and the parameter A_c is defined by the following expression [21]:

$$A_c = h_{c\infty}\left[\tau_c - 2\ln(\gamma_{\text{e}} qa) - \sum_{n=1}^{\infty} \frac{2\exp(-n\tau_c)}{n\cosh n\tau_c}\right]^{-1} \tag{7.111}$$

Note that the last two terms in the brackets in Eq. (7.111) are logarithmically divergent for $a \to 0$, that is for small distances between the two bodies; however, these two divergent terms cancel each other. To prove that we first notice that for $a \to 0$ we have $\tau_c \to a/r_c << 1$ and in such a case the sum in Eq. (7.111) can be exchanged with an integral as follows [21]:

$$\sum_{n=1}^{\infty} \frac{\exp(-n\tau_c)}{n\cosh n\tau_c} \to 2\int_{2\tau_c}^{\infty} \frac{dx}{x(\mathrm{e}^x + 1)} \to -\ln\frac{4\gamma_{\text{e}} a}{\pi r_c} \tag{7.112}$$

At the last step integration by part has been used along with the identity [77]

$$\int_0^{\infty} \frac{\mathrm{e}^x \ln x}{(\mathrm{e}^x + 1)^2} dx = \frac{1}{2}\ln\left(\frac{\pi}{2\gamma_{\text{e}}}\right) \tag{7.113}$$

Then the terms containing $\ln a$ in Eqs. (7.111) and (7.112) cancel each other for $a \to 0$ and, consequently, A_c remains finite in the same limit.

Next, introducing bipolar coordinates in Eq. (7.105) and substituting there Eq. (7.108) one can derive

$$\sin\Psi_c(L) = \frac{1}{2\pi r_c}\int_{-\pi}^{\pi} d\omega \left(\frac{\partial\zeta^{\text{in}}}{\partial\tau}\right)_{\tau=\tau_c} = \frac{A_c}{r_c} \qquad (qa)^2 << 1. \tag{7.114}$$

In the other limit, $(qa)^2 \geq 1$, one can find an expression for $\Psi_c(L)$ using the superposition approximation. In the framework of this approximation the elevation h_c of the contact line on each of two vertical cylinders can be presented in the form

$$h_c = h_{c\infty} + \Delta h_c + \left(\frac{\partial h_c}{\partial \sin \Psi_c} \right)_{r_c} (\sin\Psi_c - \sin\Psi_{c\infty}) \tag{7.115}$$

Here $h_{c\infty}$ is the elevation for $L \to \infty$ and

$$\Delta h_c = r_c \sin\Psi_{c\infty} \mathrm{K}_0(qL) \tag{7.116}$$

is the elevation created by a single cylinder at a distance L from its axis (the distance at which the second cylinder is situated); the last term in Eq. (7.115) accounts for the change in h_c due to the change in Ψ_c. Differentiating the Derjaguin's formula, Eq. (7.65), with $Q = r_c \sin\Psi_c$, one obtains

$$\left(\frac{\partial h_c}{\partial \sin \Psi_c} \right)_{r_c} = r_c \ln \frac{2}{\gamma_e q r_c} \tag{7.117}$$

Now we impose the boundary condition Eq. (7.107), which requires $h_c = h_{c\infty}$, and then the combination of Eqs. (7.115)–(7.117) yields [21]

$$\sin\Psi_c(L) = \sin\Psi_{c\infty} \left[1 - \left(\ln \frac{2}{\gamma_e q r_c} \right)^{-1} \mathrm{K}_0(qL) \right] \tag{7.118}$$

Equation (7.118) holds when the distance L between the two bodies is large enough and the second term in the brackets is small, i.e.

$$\varepsilon(L) \equiv \left(\ln \frac{2}{\gamma_e q r_c} \right)^{-1} \mathrm{K}_0(qL) << 1. \tag{7.119}$$

Equation (7.118) implies that $\Psi_c(L) < \Psi_{c\infty}$ and consequently, the interaction energy $\Delta\Omega$, given by Eq. (7.106), is negative and corresponds to attraction. The two asymptotics, Eq. (7.114) for short distances and Eq. (7.118) for long distances can be matched applying the standard procedure [see Eq. (7.38)] to the function $1/\sin\Psi_c(L)$; the resulting compound expression reads [21]:

$$\sin\Psi_c(L)=\left\{\frac{r_c}{A_c}+\left[\mathrm{K}_0(qL)-\ln\frac{2}{\gamma_e qL}\right]\frac{r_c}{h_{c\infty}}\right\}^{-1} \qquad (qr_c)^2 << 1. \qquad (7.120)$$

To achieve better accuracy in computations, it is recommended to use Eq. (7.118) when $\varepsilon(L)$ << 1, and to use Eq. (7.120) in all other cases.

The energies of capillary interaction corresponding to the two different boundary conditions, fixed slope and fixed elevation, are compared in Fig. 7.19. In the case of fixed slope the energy is calculated from Eq. (7.85), whereas in the case of fixed elevation – from Eqs. (7.106) and (7.120). To have a basis for comparison the parameters values denoted in Fig. 7.19 are taken to be the same for the two cases. As seen in the figure, in both cases $\Delta\Omega$ is negative and can have a magnitude of the order of 10^{-12} J. In other words, in both cases the interaction energy is much greater than the thermal energy kT and corresponds to attraction. The new moment is that the interaction at constant slope is stronger than the interaction at constant elevation [21].

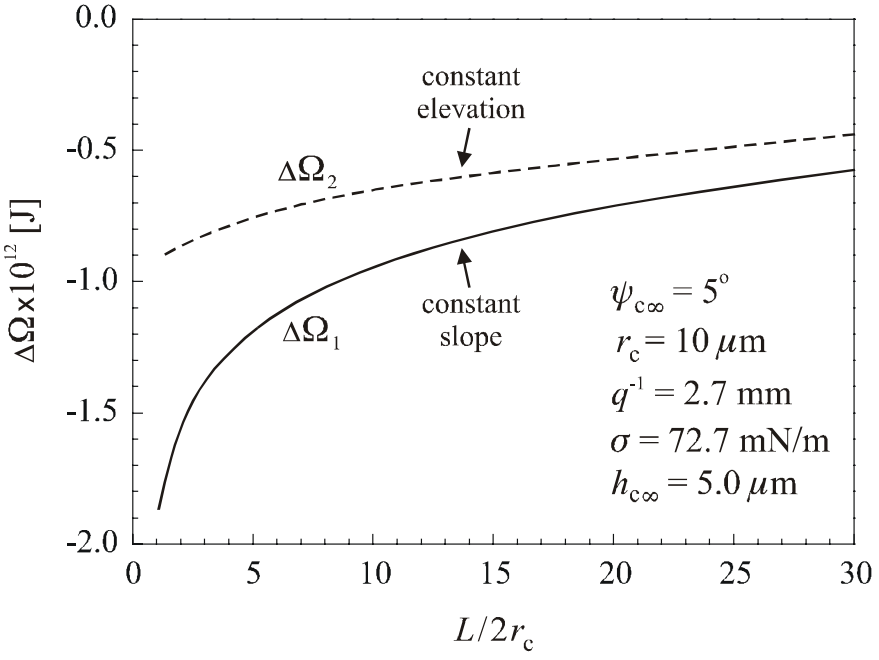

Fig. 7.19. Calculated energy of capillary attraction $\Delta\Omega$ vs. $L/2r_c$, where L is the distance between the axes of symmetry of the particles (see Fig. 7.18) and r_c is the radius of the contact line. $\Delta\Omega_1$ and $\Delta\Omega_2$ correspond to the cases of constant slope, Eq. (7.88), and constant elevation, Eq. (7.106). The values of the parameters $\Psi_{c\infty}$, r_c, q^{-1}, σ and $h_{c\infty}$ are the same for the two curves [21].

7.4. FORCE APPROACH TO THE LATERAL CAPILLARY INTERACTIONS

7.4.1. CAPILLARY IMMERSION FORCE BETWEEN TWO CYLINDERS OR TWO SPHERES

As already noted in Section 7.1.5, the lateral capillary force exerted on each of two interacting particles is a sum of the net forces due to the interfacial tension and hydrostatic pressure: $\mathbf{F}^{(k)} = \mathbf{F}^{(k\sigma)} + \mathbf{F}^{(k\mathrm{p})}$ ($k = 1,2$), see Eqs. (7.21)–(7.23). $\mathbf{F}^{(k\sigma)}$ is calculated by integration of the meniscus interfacial tension σ along the contact line, while $\mathbf{F}^{(k\mathrm{p})}$ is determined by the integral of the hydrostatic pressure P throughout the particle surface. Our purpose below is following Ref. [19] to obtain explicit analytical expressions for $\mathbf{F}^{(k\sigma)}$ and $\mathbf{F}^{(k\mathrm{p})}$, and to compare the numerical results obtained by means of the alternative force and energy approaches.

First, let us calculate the capillary force $\mathbf{F}^{(k)}$ for each of the two partially immersed vertical cylinders depicted in Fig. 7.12. It is convenient to make a special choice of the coordinate system, see Fig. 7.20. The z-axis coincides with the axis of the considered cylinder. The plane xy, as usual, coincides with the horizontal fluid interface far from the cylinders. The x-axis is directed from the cylinder of consideration toward the other cylinder. The symmetry of the system implies that the y- components of $\mathbf{F}^{(k\sigma)}$ and $\mathbf{F}^{(k\mathrm{p})}$ are equal to zero. For that reason our task is reduced to the calculation of

$$F_x^{(k\sigma)} = \mathbf{e}_x \cdot \mathbf{F}^{(k\sigma)} \qquad \text{and} \qquad F_x^{(k\mathrm{p})} = \mathbf{e}_x \cdot \mathbf{F}^{(k\mathrm{p})} \tag{7.121}$$

where $\mathbf{e}_x$ is the unit vector of the x-axis. Note that due to the specific choice of the coordinate system, the positive (negative) value of the projection $F_x^{(k)}$ corresponds to attraction (repulsion) between the two cylinders.

Force $F_x^{(k\sigma)}$ due to the interfacial tension. Let $z = \zeta(\varphi)$ be the equation of the contact line with φ being the azimuthal angle in the plane xy, see Fig. 7.20. The position vector of a point belonging to the contact line is

$$\mathbf{R}(\varphi) = \mathbf{e}_x r_k \cos\varphi + \mathbf{e}_y r_k \sin\varphi + \mathbf{e}_z \zeta(\varphi) \tag{7.122}$$

where, as usual, r_k is the radius of the contact line. The linear element along the contact line is

$$dl = \chi \, d\varphi, \qquad \chi \equiv |d\mathbf{R}/d\varphi| = [r_k^2 + (d\zeta/d\varphi)^2]^{1/2}, \tag{7.123}$$

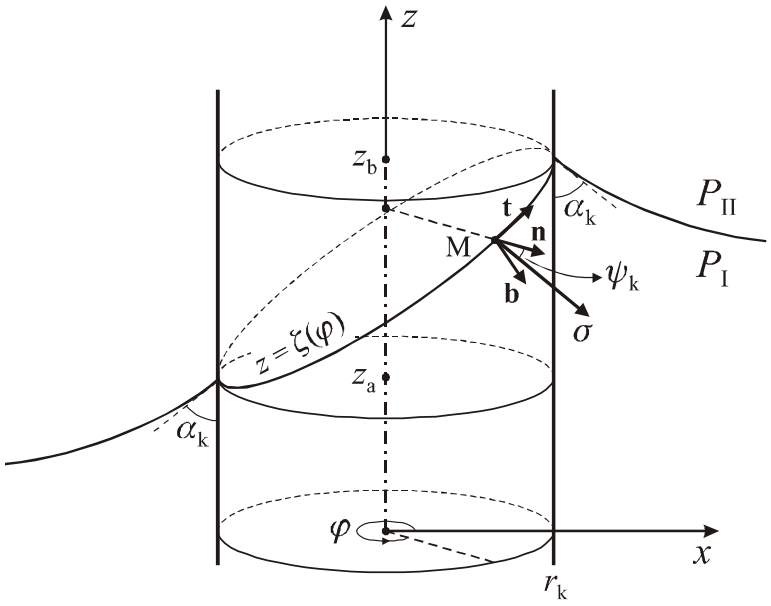

Fig. 7.20. Sketch of the capillary meniscus around one of the two cylinders depicted in Fig. 7.12; r_k is the radius of the cylinder, α_k is contact angle; $z = \zeta(\varphi)$ is the equation of the three-phase contact line with running unit tangent **t**; **n** is a running unit normal to the cylinder surface; $\mathbf{b} = \mathbf{t} \times \mathbf{n}$ is a unit binormal; **σ** is the vector of surface tension, which is perpendicular to **t**, but tangential to the meniscus surface. The slope of the contact line is exaggerated.

The vector of the running unit tangent to the contact line is

$$\mathbf{t} \equiv \frac{1}{\chi}\frac{d\mathbf{R}}{d\varphi} = \frac{1}{\chi}\left(-\mathbf{e}_x r_k \sin\varphi + \mathbf{e}_y r_k \cos\varphi + \mathbf{e}_z \frac{d\zeta}{d\varphi} \right) \tag{7.124}$$

The vector of the outer running unit normal to the cylindrical surface is (Fig. 7.20)

$$\mathbf{n} = \mathbf{e}_x \cos\varphi + \mathbf{e}_y \sin\varphi \tag{7.125}$$

At each point of the contact line (see the point *M* in Fig. 7.20) one can define the vector of the unit binormal as follows:

$$\mathbf{b} = \mathbf{t} \times \mathbf{n} \tag{7.126}$$

The vector of the interfacial tension $\underline{\boldsymbol{\sigma}}$, exerted at the contact line, is simultaneously tangential to the meniscus surface and normal to the contact line; hence $\underline{\boldsymbol{\sigma}}$ belongs to the plane formed by the vectors **n** and **b**:

$$\underline{\boldsymbol{\sigma}} = \sigma(\mathbf{b} \sin\psi_k + \mathbf{n} \cos\psi_k), \tag{7.127}$$

see Fig. 7.20. Next, we substitute Eqs. (7.124)–(7.126) into Eq. (7.127) to derive

$$\sigma_x \equiv \mathbf{e}_x \cdot \underline{\boldsymbol{\sigma}} = \sigma \left(\cos\varphi \cos\psi_k - \frac{1}{\chi} \frac{d\zeta}{d\varphi} \sin\varphi \sin\psi_k \right) \tag{7.128}$$

Combining eqs. (7.22). (7.121), (7.123) and (7.128) one obtains [19]

$$F_x^{(k\sigma)} = \oint_{L_k} dl \;\; \sigma_x = -\pi\sigma \sin\psi_k \int_0^{2\pi} \frac{d\zeta}{d\varphi} \sin\varphi d\varphi + \Delta F_x^{(k)} \tag{7.129}$$

where we have introduced the notation

$$\Delta F_x^{(k)} = \sigma \cos\psi_k \int_0^{2\pi} \chi \cos\varphi d\varphi \approx \frac{\sigma}{r_k} \int_0^{\pi} \left(\frac{d\zeta}{d\varphi} \right)^2 \cos\varphi d\varphi \tag{7.130}$$

At the last step we have used the condition for small meniscus slope, $|\nabla_{II}\zeta|^2 << 1$, and have expanded in series the square root in Eq. (7.123). Further, it is convenient to introduce parametrization of the contact line in terms of the angle ω of the bipolar coordinate system (τ, ω), see Eq. (7.25). By means of some geometrical considerations one can find the connection between ω and φ [19]:

$$\cos\varphi = \frac{1 - \cosh\tau_k \cos\omega}{\cosh\tau_k - \cos\omega}, \qquad 0 \le \varphi \le \pi, \qquad \pi \ge \omega \ge 0 \tag{7.131}$$

where τ_k is the value of the bipolar coordinate τ at the contact line, see Eq. (7.49). With the help of Eq. (7.131) one can bring Eqs. (7.129) and (7.130) into the form [19]:

$$F_x^{(k\sigma)} = 2\pi\sigma \sin\psi_k \sinh\tau_k \int_0^{\pi} \frac{d\zeta}{d\omega} \frac{\sin\omega d\omega}{\cosh\tau_k - \cos\omega} + \Delta F_x^{(k)} \tag{7.132}$$

$$\Delta F_x^{(k)} = \frac{\sigma}{a} \int_0^{\pi} \left(\frac{d\zeta}{d\omega} \right)^2 (1 - \cosh\tau_k \cos\omega) d\omega \tag{7.133}$$

In fact Eqs. (7.132)–(7.133) are the final equations for calculating $F_x^{(k\sigma)}$: one has to substitute $\zeta(\omega) = \zeta_{c,k}(\omega)$ from Eq. (7.66) and then to carry out numerically the integration in Eqs. (7.132)–(7.133). For not too large distances between the cylinders, for which $(qa)^2 << 1$, it

is better to substitute $\zeta(\omega) = \zeta_k(\tau_k, \omega)$ from Eq. (7.42); then the integration in Eq. (7.132) can be carried out analytically [19]:

$$F_x^{(k\sigma)} = 2\pi\sigma \sin\psi_k \left[Q_k \mathrm{e}^{-\tau_k} + 2(Q_1 - Q_2)(-1)^k \sinh\tau_k \sum_{n=1}^{\infty} \frac{\mathrm{e}^{-2n\tau_k} - E^{(n)}}{1 - E^{(n)}} \right] + \Delta F_x^{(k)} \qquad (7.134)$$

with $E^{(n)} \equiv \exp[-2n(\tau_1 + \tau_2)]$. However, the integral in Eq. (7.133) cannot be solved analytically and has to be calculated numerically. The calculations show that for small particles, $(qr_k)^2 << 1$, the quadratic term $\Delta F_x^{(k)}$ is only a small correction in comparison with $F_x^{(k\sigma)}$ and it is not a great loss of accuracy if the term $\Delta F_x^{(k)}$ in Eqs. (7.132) and (7.134) is neglected.

For large interparticle separations from Eq. (7.134) one can obtain a simple asymptotic formula, see Ref. [19] for details:

$$F_x^{(k\sigma)} \approx 2\pi\sigma \sin\psi_1 \sin\psi_2 \frac{r_1 r_2}{L}, \qquad (r_k/L)^2 << 1, \quad (qa)^2 << 1. \qquad (7.135)$$

Force $F_x^{(kp)}$ due to the hydrostatic pressure. To calculate $F_x^{(kp)}$ one can identify the integration surface S_k in Eq. (7.23) with the part of the cylindrical surface comprised between the horizontal planes $z = z_a$ and $z = z_b$, see Fig. (7.20). The hydrostatic pressure can be expressed in the form

$$P = \begin{cases} P_{\mathrm{I}} \text{ for } z_a \le z \le \zeta(\varphi) \\ P_{\mathrm{II}} \text{ for } \zeta(\varphi) \le z \le z_b \end{cases} \qquad (7.136)$$

where $P_Y = P_0 - \rho_Y g z$, Y = I, II is the hydrostatic pressure in the respective phase and P_0 is the pressure at level $z = 0$; as before, $\zeta(\varphi)$ is the equation of the contact line. Combining Eqs. (7.23), (7.121), (7.125) and (7.136) one derives [19]

$$F_x^{(kp)} = -\int_{-\pi}^{\pi} d\varphi r_k \cos\varphi \int_{z_a}^{z_b} dz P = \Delta\rho g r_k \int_0^{\pi} \zeta^2(\varphi) \cos\varphi d\varphi \qquad (7.137)$$

where $\Delta\rho = \rho_{\mathrm{I}} - \rho_{\mathrm{II}}$. Using Eqs. (7.29) and (7.131) one can express Eq. (7.137) into the equivalent form

$$F_x^{(kp)} = \Delta\rho g a \int_0^{\pi} \frac{1-\cosh\tau_k \cos\omega}{(\cosh\tau_k - \cos\omega)^2} \zeta^2 d\omega \tag{7.138}$$

To calculate $F_x^{(kp)}$ from Eq. (7.138) one is to substitute $\zeta = \zeta_{c,k}(\omega)$ from Eq. (7.66) [or alternatively $\zeta = \zeta_k(\tau_k, \omega)$ from Eq. (7.42)] and then to carry out numerically the integration.

The series expansion for long distances leads to the following asymptotic expression for $F_x^{(kp)}$ [19]:

$$F_x^{(kp)} \approx 2\pi\sigma (qr_k)^2 h_k r_j \sin\psi_j \frac{1}{L}, \qquad (r_k/L)^2 << 1, \quad (qa)^2 << 1. \tag{7.139}$$

$j,k = 1,2; j \neq k$. The comparison of Eqs. (7.135) and (7.139) shows that the ratio

$$F_x^{(kp)} / F_x^{(k\sigma)} \approx (qr_k)^2 \frac{h_k}{r_k \sin\psi_k} \tag{7.140}$$

is a small quantity for the case of small particles, that is for $(qr_k)^2 << 1$; indeed, the Derjaguin formula, Eq. (7.51), shows that $h_k/(r_k \sin\psi_k) \approx \ln(2/\gamma_e qr_k)$ and the latter logarithm is a quantity of the order of 1 up to 10. Thus one may conclude that for small particles, $(qr_k)^2 << 1$, $F_x^{(kp)}$ is much smaller than $F_x^{(k\sigma)}$, and therefore in a first approximation $F_x^{(kp)}$ can be neglected.

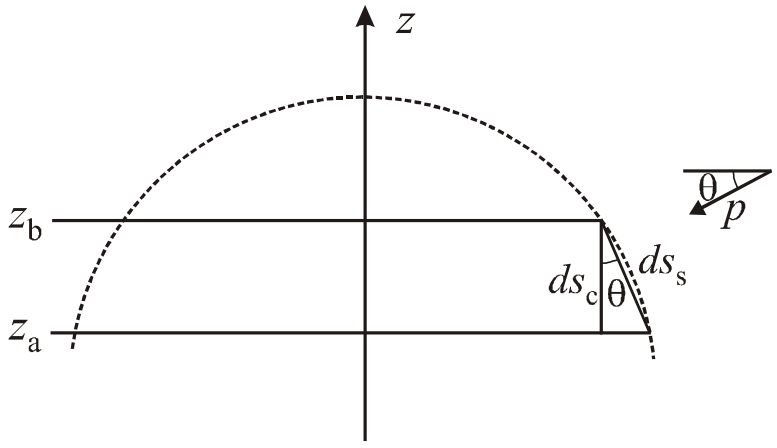

Fig. 7.21. Cross section of a spherical particle: the pressure P is directed normally to the spherical element ds_s, whose projection on the vertical cylindrical surface is denoted by ds_c.

Application to Spherical Particle. In Section 7.3.2 we demonstrated that the expression for the meniscus profile around two vertical cylinders, $\zeta(\tau, \omega)$, can be applied to approximately calculate the capillary interaction between two spheres confined in a liquid film. Similarly, when the deviation of the contact line from the horizontal position is not too large, one can combine one of Eqs. (7.42), (7.46), (7.64) or (7.66) with Eqs. (7.132) and (7.138) to calculate $F_x^{(k\sigma)}$ and $F_x^{(kp)}$. It should be taken into account that for spherical particles r_k and ψ_k depend on the distance L; the later dependence can be obtained by applying the numerical procedure based on Eqs. (7.101)–(7.102).

The applicability of Eq. (7.138) to spherical particles needs additional discussion. Let us consider an element ds_s from the surface of a sphere, whose projection on the cylindrical surface (see Fig. 7.21) is $ds_c = (ds_s)\cos\theta$. Then the horizontal projection of the force exerted on the spherical element ds_s is $P\cos\theta\, ds_s = Pds_c$. Note also that z_a and z_b in Fig. 7.21 are the same as in Fig. 7.20. Hence the integration over the spherical belt can be replaced by an integration over the portion of the cylindrical surface comprised between the planes $z = z_a$ and $z = z_b$. In other words, Eq. (7.137), and its corollary (7.138), can be used also in the case of spherical particle.

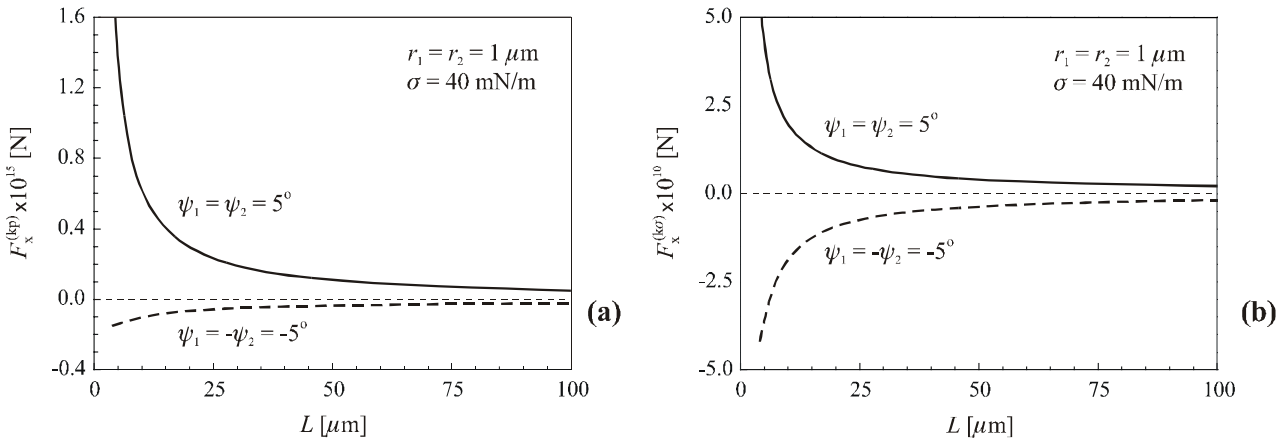

Fig. 7.22. Calculated in Ref. [19] plots of capillary force vs. distance L between two semi-immersed vertical cylinders of equal radii, $r_1 = r_2 = 1$ μm at various contact angles: (a) contribution of the hydrostatic pressure, $F_x^{(kp)}$, calculated from Eq. (7.138); (b) contribution of surface tension, $F_x^{(k\sigma)}$, calculated from Eq. (7.134).

Numerical results and discussion. Figure 7.22 shows plots of the calculated $F_x^{(k\sigma)}$ and $F_x^{(kp)}$ vs. the distance L between the axes of two vertical cylinders of radii $r_1 = r_2 = 1$ μm. $F_x^{(k\sigma)}$ is calculated from Eq. (7.134) while $F_x^{(kp)}$ is calculated by means of Eqs. (7.138) and (7.46). The other parameters values are $\sigma = 40$ mN/m and $|\psi_1| = |\psi_2| = 5°$. Figure 7.22 illustrates the fact that the lateral capillary forces can be either attractive or repulsive depending on the sign of the angles ψ_1 and ψ_2, cf. Fig. 7.1. The numerical results for $F_x^{(kp)}$ and $F_x^{(k\sigma)}$, shown in Fig. 7.22a and 7.22b confirm the conclusion drawn from Eq. (7.140) that for small particles, $(qr_k)^2 << 1$, the force $F_x^{(kp)}$ due to the hydrostatic pressure is much smaller than the force $F_x^{(k\sigma)}$ due to the interfacial tension. For the numerical example shown in Fig. 7.22 $F_x^{(kp)}$ is with 5 orders of magnitude smaller than $F_x^{(k\sigma)}$.

Table 7.1 contains numerical data calculated for two vertical cylinders of *different* radii ($r_1 =$ 10 μm and $r_2 = 30$ μm) and different contact angles ($\psi_1 = 10°$ and $\psi_2 = 1°$). The capillary immersion force $F_x^{(k)} = F_x^{(k\sigma)} + F_x^{(kp)}$ is calculated by means of Eqs. (7.133), (7.134) and (7.138). If the approximations used to derive the latter equations are correct one should obtain $F_x^{(1)} = F_x^{(2)}$ (the third Newton's law), irrespective of the fact that the two cylinders have different radii and contact angles. The data in Table 7.1 for $F_x^{(1)}$ and $F_x^{(2)}$ really confirm the validity of the employed approximations.

Moreover, the force and energy approaches must be equivalent, that is

$$F_x^{(1)} = F_x^{(2)} = \frac{d(\Delta\Omega)}{dL} \tag{7.141}$$

In other words the differentiation of Eq. (7.88) [or Eq. (7.89)], expressing $\Delta\Omega$, should give the same values of the force as the integral expressions, Eqs. (7.133), (7.134) and (7.138), obtained by means of the force approach. The numerical data in Table 7.1 confirm that Eq. (7.141) is satisfied with a very good accuracy, irrespective of the differences in the procedures and the approximations used to calculate $F_x^{(1)}$ and $F_x^{(2)}$ in the force approach and $d(\Delta\Omega)/dL$ in the energy approach. Note, for example, that in the energy approach we have worked in terms of the average elevation of the contact line, h_k, just as if the contact lines were horizontal, see

Eq. (7.88), whereas in the force approach the inclination of the contact line, $d\zeta/d\varphi$, plays a central role; indeed Eqs. (7.129), (7.130) and (7.137) give zero force if $d\zeta/d\varphi$ is set zero.

Table 7.1. Comparison of the calculated values of $F_x^{(1)}, F_x^{(2)}$ and $d(\Delta\Omega)/dL$ for $r_1 = 10$ μm, $r_2 = 30$ μm, $\psi_1 = 10°$ and $\psi_2 = 1°$ for various values of the distance L between the axes of two vertical cylinders, partially immersed in a liquid of surface tension $\sigma = 40$ mN/m.

$s = L/2$ [μm]	$F_x^{(1)}$ [N]	$F_x^{(2)}$ [N]	$d(\Delta\Omega)/dL$ [N]
50	1.482×10^{-8}	1.485×10^{-8}	1.483×10^{-8}
100	3.054×10^{-9}	3.061×10^{-9}	3.054×10^{-9}
150	1.737×10^{-9}	1.742×10^{-9}	1.737×10^{-9}
200	1.231×10^{-9}	1.234×10^{-9}	1.231×10^{-9}
250	9.590×10^{-10}	9.612×10^{-10}	9.588×10^{-10}
300	7.876×10^{-10}	7.893×10^{-10}	7.875×10^{-10}
350	6.692×10^{-10}	6.706×10^{-10}	6.691×10^{-10}
400	5.822×10^{-10}	5.834×10^{-10}	5.821×10^{-10}
450	5.155×10^{-10}	5.165×10^{-10}	5.154×10^{-10}
500	4.626×10^{-10}	4.635×10^{-10}	4.625×10^{-10}

The data in Table 7.1 confirm *numerically* the equivalence of the force and energy approaches to the calculation of the lateral capillary forces. One can find an *analytical* proof of this equivalence in Ref. [21] for the case of two vertical cylinders.

7.4.2. ASYMPTOTIC EXPRESSION FOR THE CAPILLARY FORCE BETWEEN TWO PARTICLES

In Section 7.1.3 we derived the asymptotic formula $F \approx -2\pi\sigma Q_1 Q_2 q \mathrm{K}_1(qL)$ for the capillary force by using the *energy* approach, see Eq. (7.13). Our purpose here is to demonstrate that the *force* approach yields the same asymptotic formula.

Our starting point is Eq. (7.66), which describes the shape of the contact line on a vertical cylinder (and in first approximation – on a spherical particle as well). We expand Eq. (7.66) in series for $r_k/s_k << 1$, which means that we seek the shape of the contact line at relatively long distances between the two particles (then $s_1 \approx s_2 \approx a \approx L/2$):

$$\zeta_k(\omega) = h_{k\infty} + Q_j[\mathrm{K}_0(qL) - 2r_k\, q\mathrm{K}_1(qL)\cos\omega + ...] \qquad (j,k = 1,2; j \neq k) \qquad (7.142)$$

Differentiating Eq. (7.142) one obtains

$$\frac{d\zeta_k}{d\omega} \approx 2r_k Q_j\, qK_1(qL)\sin\omega \qquad (j,k = 1,2; j \neq k) \qquad (7.143)$$

Since for small particles, that is for $(qr_k)^2 << 1$, the terms $\Delta F_x^{(k)}$ and $F_x^{(kp)}$ represent only small corrections in the expression for the capillary force, then the force is given with a good accuracy by the integral term in Eq. (7.132):

$$F_x^{(k)} \approx 2\pi\sigma \sin\psi_k \sinh\tau_k \int_0^{\pi} \frac{d\zeta_k}{d\omega} \frac{\sin\omega\, d\omega}{\cosh\tau_k - \cos\omega} \qquad (7.144)$$

Next, we substitute Eq. (7.143) into Eq. (7.144) to obtain the sought for asymptotic formula [64]:

$$F_x \approx 2\sigma Q_1 Q_2 qK_1(qL)\sinh\tau_2 \int_{-\pi}^{\pi} \frac{\sin^2\omega\, d\omega}{\cosh\tau_2 - \cos\omega} \approx 2\pi\sigma Q_1 Q_2 qK_1(qL) \qquad (7.145)$$

(the choice of the coordinate system in Fig. 7.20 implies that $F_x > 0$ corresponds to attraction).

At the last step we have used the fact that $Q_k \equiv r_k \sin\psi_k$, the identity [19]

$$\int_{-\pi}^{\pi} \frac{\sin^2\omega\, d\omega}{\cosh\tau_2 - \cos\omega} = 2\pi \exp(-\tau_2) \qquad (7.146)$$

and the approximation

$$2\sinh\tau_2 \exp(-\tau_2) \approx 1 \qquad \text{for} \qquad \tau_2 \geq 2 \qquad (r_2/s_2 << 1) \qquad (7.147)$$

see also Eq. (7.29).

As could be expected, the derived asymptotic expression for the lateral capillary force, Eq. (7.145), is identical to Eq. (7.13), both of them corresponding to the boundary condition of fixed contact angle. Note that during the derivation of Eq. (7.145) it was not necessary to specify whether the capillary force is of flotation or immersion type, or whether we deal with a single interface or with a thin liquid film. We have used only the integral expression for the capillary force, Eq. (7.144), which is valid in all aforementioned cases, as well as Eq. (7.66) for the shape of the contact line. The latter equation accounts for the overlap of the interfacial

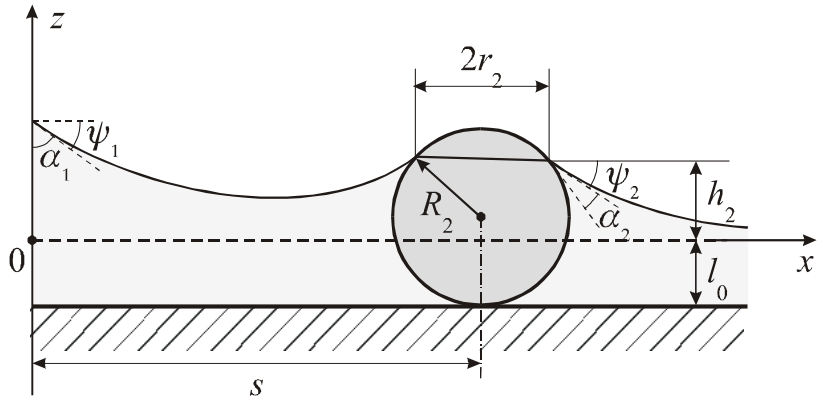

Fig. 7.23. Sketch of the capillary meniscus around a spherical particle, which is situated at a distance s from a vertical wall. The particle is confined in a liquid film whose thickness is uniform and equal to l_0 far from the particle and the wall; R_2 and r_2 are the radii of the particle and its contact line; α_1 and α_2 are three-phase contact angles; ψ_1 and ψ_2 are meniscus slope angles; h_2 is the capillary elevation of the contact line at the particle surface.

deformations created by the two particles (cylinders) irrespective of the origin of the deformation: weight of the particle or capillary rise (wetting). Consequently, the above derivation of the expression for the capillary interaction by means of the force approach once again confirms the general conclusion that all kind of lateral capillary forces are due to the overlap of perturbations in the interfacial shape created by attached bodies.

Note that Eq. (7.145) is an approximate asymptotic formula, which is valid for comparatively long distances between the particles ($L >> r_1, r_2$). For not-too-long distances the more accurate analytical expressions for the capillary force from Sections 7.3 and 7.4.1 have to be used.

7.4.3. CAPILLARY IMMERSION FORCE BETWEEN SPHERICAL PARTICLE AND WALL

In this section following Ref. [18] we consider another configuration: a planar vertical wall and a planar horizontal substrate covered with a liquid layer, which has thickness equal to l_0 far from the wall. Our aim is to determine the lateral capillary force between the wall and a sphere, which is partially immersed in the liquid film, see Fig. 7.23. As usual, the coordinate plane xy is chosen to coincide with the horizontal upper surface of the liquid layer far from the sphere and the wall. In addition, the x-axis is oriented perpendicular to the vertical wall. The geometric parameters related to the wall are denoted by subscript 1, whereas those related to the particle – by subscript 2, see Fig. 7.23 for the notation.

Following an approach analogous to that from Section 7.2.1 one can find a compound asymptotic solution for the shape of the meniscus in Fig. 7.23 assuming that the meniscus slope is small, i.e. $|\nabla_{II}\zeta|^2 << 1$. The compound solution, obtained in terms of the bipolar coordinates, Eq. (7.25), reads [18]:

$$\zeta(\tau, \omega) = q^{-1}\cot\alpha_1 \, e^{-qx} + Q_2 \{2K_0(qr) + \ln[(\cosh\tau - \cos\omega)r^2/(2a^2)]\}, \qquad x \geq 0; \quad (7.148)$$

here, as usual, $Q_2 = r_2 \sin\psi_2$ and $r = (x^2 + y^2)^{1/2}$. In particular, Eq. (7.148) allows one to determine the shape of the contact line on the wall [18],

$$\zeta_1(y) \equiv q^{-1}\cot\alpha_1 + Q_2 [2K_0(|qy|) + \ln(1 - a^2/y^2)], \quad (7.149)$$

as well as the increase of the wet area on the wall due to the presence of the spherical particle:

$$\Delta A \equiv \int_{-\infty}^{+\infty} [\zeta_1(y) - \zeta_1(\infty)]dy = 2\pi q^{-1} Q_2 (1 - qa) \quad (7.150)$$

The form of Eq. (7.148) shows that if the contact angle at the wall is $\alpha_1 = 0$, then the shape of the meniscus is the same as that of the meniscus around two identical particles separated at a distance s, each of them being the mirror image of the other one with respect to the wall. For that reason in such a case the capillary interaction between particle and wall is equivalent to the interaction of the particle with its mirror image. In this aspect there is an analogy with the image forces in electrostatics; the same analogy is present also in the case of floating particle, see Chapter 8 below.

In the considered case of small meniscus slope the projection of the particle contact line on the plane xy can be approximately considered as a circumference of radius r_2. When the distance s between the particle and the wall varies, then both r_2 and ψ_2 alter. The values of r_2, ψ_2 and of the meniscus elevation at the particle contact line, h_2, can be determined for each given s by solving numerically the equation [18]

$$h_2 = q^{-1}\cot\alpha_1 \exp(-qs) - r_2 \sin\psi_2 \ln[(\gamma_e q)^2 (s + a) r_2 /4], \quad (7.151)$$

in which r_2 and ψ_2 are expressed as functions of h_2 as follows:

$$r_2(h_2) = [(l_0 + h_2)(2R_2 - l_0 - h_2)]^{1/2}, \qquad \psi_2(h_2) = \arcsin(r_2(h_2)/R_2) - \alpha_2 ,$$

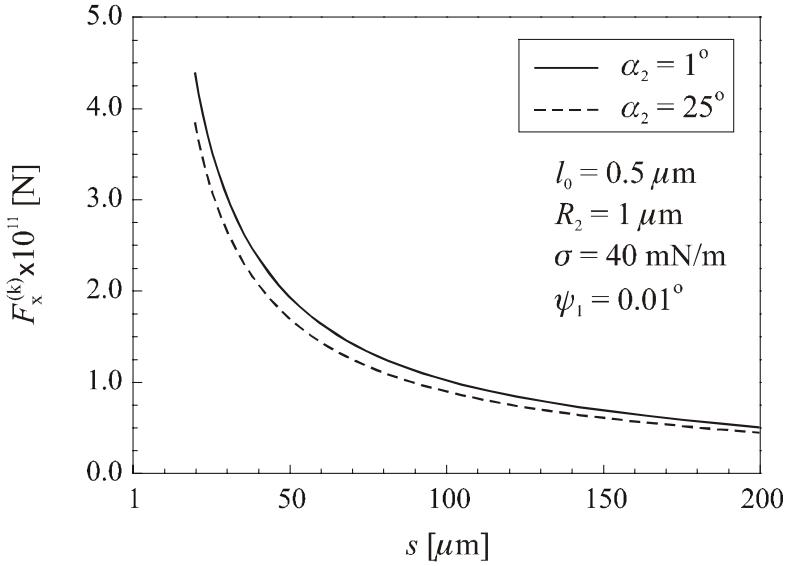

Fig. 7.24. Calculated in Ref. [18] capillary force, $F_x^{(k)} = F_x^{(k\sigma)} + F_x^{(kp)}$, exerted on a particle of radius R_2 = 1 μm which is situated at a distance s from a vertical wall, see Fig. 7.23. The two curves correspond to particle contact angles α_2 = 1° and 25°; the other parameter values are: l_0 = 0.5 μm, σ = 40 mN/m and ψ_1 = 0.01°.

cf. Eqs. (7.92) and (7.99). The values of the geometrical parameters thus determined can be further used to calculate the force of particle-wall interaction. The contributions of the meniscus surface tension and the hydrostatic pressure, $F_x^{(k\sigma)}$ and $F_x^{(kp)}$, can be calculated substituting Eq. (7.148) for $\tau = \tau_2 = \ln[(s + a)/r_2]$ into Eqs. (7.132)–(7.133) and (7.138) and carrying out numerically the integration with respect to ω.

As an illustration Fig. 7.24 presents the calculated force $F_x^{(k)} = F_x^{(k\sigma)} + F_x^{(kp)}$ plotted against the particle-to-wall distance s; the two curves correspond to two values of the particle contact angle: α_2 = 1° and 25°. The other parameter values are R_2 = 1 μm, ψ_1 = 0.01° and l_0 = 0.5 μm. The calculated capillary force (Fig. 7.24) corresponds to attraction between the spherical particle and the wall.

7.5. SUMMARY

Lateral capillary forces appear when the contact of particles (or other bodies) with a fluid phase boundary brings about perturbations in the interfacial shape. The capillary interaction is due to the overlap of such perturbations. The latter can appear around floating particles (Fig. 7.1a,c), particles confined in a liquid film (Figs. 7.1b,d,f), particles attached to holders (Fig. 7.7),

vertical cylinders (Fig. 7.10), inclusions in lipid membranes (Fig. 7.18c), etc., and can be both attractive (between similar particles) and repulsive (between dissimilar particles). The asymptotic law of the capillary interaction, Eq. (7.13) or Eq. (7.145), in its approximate form given by Eq. (7.14), resembles the Coulomb's law in electrostatics. Following the latter analogy one can introduce "capillary charges" of the attached particles (see Eq. 7.9), which can be both positive and negative. Except the case of floating particles (see Chapter 8), whose weight causes the meniscus deformations, in all other cases the deformations are governed by the surface wetting properties of partially immersed bodies or particles. The resulting "immersion" capillary forces can be large enough (Fig. 7.15) to cause two-dimensional aggregation and ordering of small colloidal particles, which has been observed in many experiments.

There are two equivalent theoretical approaches to the lateral capillary interactions: energy and force approaches. Both of them require the Laplace equation of capillarity to be solved and the meniscus profile around the particles to be determined, see Section 7.2.1. The energy approach accounts for contributions due to the alteration of the meniscus area, gravitational energy and/or energy of wetting, see Eq. (7.16). The second approach is based on calculating the net force exerted on the particle which can originate from the hydrostatic pressure and interfacial tension, see Eqs. (7.21)–(7.23) and (7.132)–(7.138). In the case of small overlap of the interfacial perturbations created by two interacting bodies, the superposition approximation can be combined with the energy or force approach to derive an asymptotic formula for the lateral capillary force, see Sections 7.1.3 and 7.4.2. This formula has been found to agree well with the experiment (Figs. 7.5 and 7.8).

Using the method of the matched asymptotic expansions one can derive analytical expressions for the capillary elevation of the contact line, h_k, and the shape of the contact line, $\zeta_{c,k}(\omega)$, see Sections 7.2.2 and 7.2.3. The energy of capillary immersion interaction between *two vertical cylinders* turns out to be equal to a half of the energy of wetting and can be expressed in terms of h_k, cf. Eqs. (7.83) and (7.84). The expression for the energy of interaction between *two spherical particles*, Eq. (7.98), is similar, but it should be taken into account that the radius of the contact lines on the particles alters when the interparticle distance is varied, see

Eqs. (7.99)–(7.102). In a similar way one can calculate the energy of capillary interaction between *cylinder and sphere*, see Eq. (7.104) and Fig. 7.17.

The energy approach has been also applied to the case, when the position of the contact line (rather than the magnitude of the contact angle) is fixed at the particle surface (Section 7.3.4). This can happen when the contact line is attached to some edge, or to the boundary between hydrophilic and hydrophobic zones on the particle surface, see Fig. 7.18. The derived analytical expressions, Eqs. (7.106) and (7.120), predict that the capillary interaction at fixed meniscus *elevation* is weaker than that at fixed meniscus *slope*; however in both cases it corresponds to attraction between similar bodies and its energy can be much larger than the thermal energy kT, see Fig. 7.19.

For small particles, that is for $(qr_k)^2 << 1$, the contribution of the hydrostatic pressure to the capillary force is found to be negligible (Eq. (7.140) and Fig. 7.21) and one can calculate the capillary force from Eq. (7.132), which represents a contribution from the interfacial tension. The latter expression, can be employed also to calculate the capillary immersion force between *particle and wall*, see Section 7.4.3. A test of the theoretical expressions for the capillary force, stemming from the alternative energy and force approaches, show that they are in a very good numerical agreement (Table 7.1).

In conclusion, the capillary immersion forces can appear in a variety of systems with characteristic particle size from 1 cm down to 2 nm (see Fig. 8.3 below); in all cases the lateral capillary interaction has a similar origin (overlap of interfacial deformations created by the particles) and is subject to a unified theoretical treatment.

7.6. REFERENCES

1. D.F. Gerson, J.E. Zaijc, M.D. Ouchi, in: M. Tomlinson (Ed.) “Chemistry for Energy”, ACS Symposium Series, Vol. 90, p.66, Amer. Chem. Soc., Washington DC, 1979.
2. J.D. Henry, M.E. Prudich, K.R. Vaidyanathan, Sep. Purif. Methods 8 (1979) 81.
3. M.M. Nicolson, Proc. Cambridge Philos. Soc. 45 (1949) 288.
4. K. Hinsch, J. Colloid Interface Sci. 92 (1983) 243.
5. C. Allain, B. Jouhier, J. Phys. Lett. 44 (1983) L421.

6. C. Allain, M. Cloitre, in: R. Jullien et al. (Eds.), Springer Proceedings in Physics, Vol. 32, Springer Verlag, Berlin, 1988, p.146.
7. B.V. Derjaguin, V.M. Starov, Colloid J. USSR Engl. Trans. 39 (1977) 383.
8. H. Yoshimura, S. Endo, M. Matsumoto, K. Nagayama, Y. Kagawa, J. Biochem. 106 (1989) 958.
9. H. Yoshimura, M. Matsumoto, S. Endo, K. Nagayama, Ultramicroscopy 32 (1990) 265.
10. L. Haggerty, B.A. Watson, M.A. Barteau, A.M. Lenhoff, J. Vac. Sci. Technol. B9 (1991) 1219.
11. N.D. Denkov, O.D. Velev, P.A. Kralchevsky, I.B. Ivanov, H. Yoshimura, K. Nagayama, Langmuir 8 (1992) 3183.
12. N.D. Denkov, O.D. Velev, P.A. Kralchevsky, I.B. Ivanov, H. Yoshimura, K. Nagayama, Nature (London) 361 (1993) 26.
13. C.D. Dushkin, K. Nagayama, T. Miwa, P.A. Kralchevsky, Langmuir 9 (1993) 3695.
14. P.A. Kralchevsky, V.N. Paunov, I.B. Ivanov, K. Nagayama, J. Colloid Interface Sci. 151 (1992) 79.
15. W.A. Gifford, L.E. Scriven, Chem. Eng. Sci. 26 (1971) 287.
16. M.A. Fortes, Can. J. Chem. 60 (1982) 2889.
17. D.Y.C. Chan, J.D. Henry, L.R. White, J. Colloid Interface Sci. 79 (1981) 410.
18. V.N. Paunov, P.A. Kralchevsky, N.D. Denkov, I.B. Ivanov, K. Nagayama, Colloids Surf. 67 (1992) 138.
19. P.A. Kralchevsky, V.N. Paunov, N.D. Denkov, I.B. Ivanov, K. Nagayama, J. Colloid Interface Sci. 155 (1993) 420.
20. V.N. Paunov, P.A. Kralchevsky, N.D. Denkov, K. Nagayama, J. Colloid Interface Sci. 157 (1993) 100.
21. P.A. Kralchevsky, K. Nagayama, Langmuir 10 (1994) 23.
22. P.A. Kralchevsky, V.N. Paunov, N.D. Denkov, K. Nagayama, J. Colloid Interface Sci. 167 (1994) 47.
23. O.D. Velev, N.D. Denkov, P.A. Kralchevsky, V.N. Paunov, K. Nagayama, J. Colloid Interface Sci. 167 (1994) 66.
24. P.A. Kralchevsky, V.N. Paunov, K. Nagayama, J. Fluid. Mech. 299 (1995) 105.
25. P.A. Kralchevsky, V.N. Paunov, N.D. Denkov, K. Nagayama, J. Chem. Soc. Faraday Trans. 91 (1995) 3415.
26. C.D. Dushkin, H. Yoshimura, K. Nagayama, Chem. Phys. Lett. 204 (1993) 455.
27. G.S. Lazarov, N.D. Denkov, O.D. Velev, P.A. Kralchevsky, K. Nagayama, J. Chem. Soc. Faraday Trans. 90 (1994) 2077.
28. A.S. Dimitrov, C.D. Dushkin, H. Yoshimura, K. Nagayama, Langmuir 10 (1994) 432.

29. M. Yamaki, J. Higo, K. Nagayama, Langmuir 11 (1995) 2975.
30. K. Nagayama, S. Takeda, S. Endo, H. Yoshimura, Jap. J. Appl. Phys. 34 (1995) 3947.
31. C.A. Johnson, A.M. Lenhoff, J. Colloid Interface Sci. 179 (1996) 587.
32. M. Sasaki, K. Hane, J. Appl. Phys. 80 (1996) 5427.
33. N.D. Denkov, H. Yoshimura, K. Nagayama, Phys. Rev. Lett. 76 (1996) 2354.
34. N.D. Denkov, H. Yoshimura, K. Nagayama, Ultramicroscopy 65 (1996) 147.
35. F. Burmeister, C. Schäfle, T. Matthes, M. Bohmisch, J. Boneberg, P. Leiderer, Langmuir 13 (1997) 2983.
36. H. Du, P. Chen, F. Liu, F.-D. Meng, T.-J. Li, X.-Y. Tang, Materials Chem. Phys. 51 (1997) 277.
37. S. Rakers, L.F. Chi, H. Fuchs, Langmuir 13 (1997) 7121
38. S. Matsushita, T. Miwa, A. Fujishima, Langmuir 13 (1997) 2582.
39. J. Boneberg, F. Burmeister, C. Schafle, P. Leiderer, D. Reim, A. Fery, S. Herminghaus, Langmuir 13 (1997) 7080.
40. P.C. Ohara, J.R. Heath, W.M. Gelbart, Angew. Chem. Int. Ed. Engl. 36 (1997) 1078.
41. N. Bowden, A. Terfort, J. Carbeck, G.M. Whitesides, Science 276 (1997) 233.
42. S.V. Kukhtetskii, L.P. Mikhailenko, Doklady Academii Nauk 357 (1997) 616.
43. H. Shibata, H. Yin, T Emi, Philos. Trans. Roy. Soc. London A 356 (1998) 957.
44. F. Burmeister, C. Schäfle, B. Keilhofer, C. Bechinger, J. Boneberg, P. Leiderer, Adv. Mater. 10 (1998) 495.
45. K.P. Velikov, F. Durst, O.D. Velev, Langmuir 14 (1998) 1148.
46. H. Aranda-Espinoza, A. Berman, N. Dan, P. Pincus, S. Safran, Biophys. J. 71 (1996) 648.
47. M.Ge, J.H. Freed, Biophys. J. 76 (1999) 264.
48. T. Gil, J.H. Ipsen, O.G. Mouritsen, M.C. Sabra, M.M. Sperotto, M. Zuckermann, "Theoretical Analysis of Protein Organization in Lipid Membranes", BBA - Reviews on Biomembranes, Vol. 1376 (3), Elsevier, Amsterdam, 1998; pp. 245-266.
49. C. Allain, M Cloitre, J. Colloid Interface Sci. 157 (1993) 261.
50. C. Allain, M Cloitre, J. Colloid Interface Sci. 157 (1993) 269.
51. C.M. Mate, V.J. Novotny, J. Chem. Phys. 94 (1991) 8420.
52. M.L. Forcada, M.M. Jakas, A. Gras-Marti, J. Chem. Phys. 95 (1991) 706.
53. A. Marmur, Langmuir 9 (1993) 1922.
54. G. Debregeas, F. Brochard-Wyart, J. Colloid Interface Sci. 190 (1997) 134.
55. O.P. Behrend, F. Oulevey, D. Gourdon, E. Dupas, A.J. Kulik, G. Gremaud, N.A. Burnham, Applied Physics A 66 (1998) S219.

56. H. Suzuki, S. Mashiko, Applied Physics A 66 (1998) S1271.

57. J. Lucassen, Colloids Surf. 65 (1992) 131.

58. B.V. Derjaguin, Kolloidn. Zh. 17 (1955) 207.

59. I.B. Ivanov, P.A. Kralchevsky, in: I.B. Ivanov (Ed.) Thin Liquid Films, Marcel Dekker, New York, 1988, p. 49.

60. P.A. Kralchevsky, K.D. Danov, N.D. Denkov, Chemical Physics of Colloid Systems and Interfaces, in: K.S. Birdi (Ed.) Handbook of Surface and Colloid Chemistry, CRC Press, Boca Raton, 1997.

61. E. Janke, F. Emde, F. Lösch, Tables of Higher Functions, McGraw-Hill, New York, 1960.

62. M. Abramowitz, I.A. Stegun, Handbook of Mathematical Functions, Dover, New York, 1965.

63. G.A. Korn, T.M. Korn, Mathematical Handbook, McGraw-Hill, New York, 1968.

64. P.A. Kralchevsky, K. Nagayama, Adv. Colloid Interface Sci. 85 (2000) 145.

65. H.B. Dwight, Tables of Integrals and Other Mathematical Data, Macmillan Co., New York, 1961.

66. C. Camoin, J.F. Roussell, R. Faure, R. Blanc, Europhys. Lett. 3 (1987) 449.

67. O.D. Velev, N.D. Denkov, V.N. Paunov, P.A. Kralchevsky, K. Nagayama, Langmuir 9 (1993) 3702.

68. C.D. Dushkin, P.A. Kralchevsky, H. Yoshimura, K. Nagayama, Phys. Rev. Lett. 75 (1995) 3454,

69. C.D. Dushkin, P.A. Kralchevsky, V.N. Paunov, H. Yoshimura, K. Nagayama, Langmuir 12 (1996) 641.

70. P.A. Kralchevsky, C.D. Dushkin, V.N. Paunov, N.D. Denkov, K. Nagayama, Prog. Colloid Polymer Sci. 98 (1995) 12.

71. About the measurement of the gravitational constant by H. Cavendish see Rose et al., Phys. Rev. Lett. 23 (1969) 655.

72. P.A. Kralchevsky, I.B. Ivanov, J. Colloid Interface Sci. 137 (1990) 234.

73. A.H. Nayfeh, Perturbation Methods, Wiley, New York, 1973.

74. B.V. Derjaguin, Dokl. Akad. Nauk SSSR 51 (1946) 517.

75. A.J. McConnell, Application of Tensor Analysis, Dover, New York, 1957.

76. R. Hooke, T.A. Jeeves, J. Assoc. Comp. Mach. 8 (1961) 212.

77. A.P. Prudnikov, Y.A. Brychkov, O.I. Marichev, Integrals and Series, Nauka, Moscow, 1981; in Russian.